Flavour dependent study of effects of multiple parton interactions and color reconnection on the jets in high multiplicity pp collisions at $\sqrt{s} = 13$ TeV

M.Sc. THESIS

by

Anurag

(Roll No.- 2103151002)

to

DEPARTMENT OF PHYSICS
INDIAN INSTITUTE OF TECHNOLOGY
INDORE - 453552, INDIA

may, 2023

Flavour dependent study of effects of multiple parton interactions and color reconnection on the jets in high multiplicity pp collisions at $\sqrt{s} = 13$ TeV

A THESIS

Submitted in partial fulfilment of the

requirements for the award of the degree

of

Master of Science

by

Anurag

DISCIPLINE OF PHYSICS

INDIAN INSTITUTE OF TECHNOLOGY INDORE

may, 2023

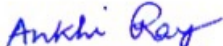**INDIAN INSTITUTE OF TECHNOLOGY**

INDORE

CANDIDATE'S DECLARATION

I hereby certify that the work which is being presented in the thesis entitled in the partial fulfillment of the requirements for the award of the degree of **Master of Science** and submitted in the **Discipline of Physics, Indian Institute of Technology Indore**, is an authentic record of my own work carried out during the time period from July 2022 to may 2023 under the supervision of **Prof. Ankhi Roy, Indian Institute of Technology Indore.**
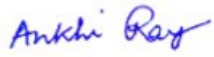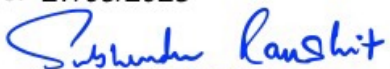
The matter presented in this thesis has not been submitted by me for the award of any other degree of this or any institute.

अनुराग

Signature of the student with date

31. 05. 2023 **(Anurag)**

- -

This is to certify that the above statement made by the candidate is correct to the best of my knowledge.

Ankhi Roy   27/05/2023

Signature of the Thesis Supervisor (with date)

(Prof. Ankhi Roy)

- -

Anurag has successfully given his M.Sc. Oral Examination held on 19/5/2023

Ankhi Roy

Signature of Thesis Supervisor

Date: 27/05/2023

Signature of PSPC Member no. 1

Date: May 27, 2023

Subhendu Rakshit

Acting Convener, DPGC

Date: 31/05/2023

Signature of PSPC Member no. 2

Date: 28/05/23

- -

Acknowledgement

First and foremost, I would like to express my deep sense of gratitude and thanks to my research supervisor **Prof. Ankhi Roy** for her guidance and for sharing her immense knowledge at time to time. I am very thankful for her constant support, immense patience, motivation and stimulating discussions which helped me a lot throughout my research.

I would also like to express my sincere respect and gratitude to my PSPC members **Prof. Subhendu Rakshit** and **Dr. Debajyoti Sarkar** for their support and crucial and thoughtful comments.

I would like to thank **DST-INSPIRE** program of the Government of India for financial support.

I am immensely indebted to **Mr. Prottoy Das**, from the Department of Physics, Bose Institute, Kolkata, for his extremely crucial remarks and guidance related to my work.

I am extremely thankful to **Mr. Sumit Kundu, Mr. Ravindra Singh, Mr. Yoshini Bailung, Swapnesh Khade** for their encouragement and crucial discussions and support. I am also thankful to all my classmates and friends who have helped me throughout my academic journey here at IIT Indore.

Last but not least, I would like to thank my parents who have made it possible for me to pursue my dreams and aspirations and who have guided me in all aspects of my life.

<div align="right">

Anurag
M.Sc., Final year
Discipline of Physics
IIT Indore

</div>

Abstract

This thesis presents a flavor-dependent study of the effects of multiparton interactions (MPI) and color reconnection (CR) on the properties of jets in high multiplicity proton-proton (pp) collisions at a center-of-mass energy of 13 TeV. The study is performed using Monte Carlo simulations based on the Pythia 8 event generator, with the effects of multiple parton interactions and color reconnection implemented using the corresponding models in Pythia 8. Both multiple parton interactions and color reconnection significantly affect the properties of jets in pp collisions at high multiplicity. It is found that multiple parton interactions lead to an increase in the number of final state particles and also affect the distribution of transverse momentum and energy of the particles inside the jet. Color reconnection also leads to a modification of the jet shape.

The jet shape modification also depends on the flavor and transverse momentum of the initiator parton of the jet. It is found that the effects of multiple parton interactions (MPI) and color reconnection (CR) are more pronounced for low transverse momenta (p_T) jets compared to high p_T jets. These effects reflect in Several experimental observables such as the suppression in nuclear modification factor R_{AA}, modification of differential jet shape observable $\rho(r)$, etc.

In this work, The modification of $\rho(r)$ in the presence of MPI and CR is presented for inclusive jets as well as for different-different flavor initiated jets in two jet transverse momentum ranges $10 < p_{T,jet} < 20 GeV/c$, $50 < p_{T,jet} < 120 GeV/c$. The results of this study are important for understanding the underlying physics of different parton-initiated jet production and their interactions with the partonic medium in high-multiplicity pp collisions.

Contents

List of Figures

iii

Chapter 1

1 Introduction

Experimental observations at RHIC and LHC have revealed that in heavy ion collisions, a high-density and high-temperature state of matter is produced, which is believed to be a deconfined state of quarks and gluons, known as Quark-Gluon Plasma (QGP) [4] [2] [9]. QGP is a state of matter where quarks and gluons are no longer confined within hadrons but can move freely over a large volume of space. The formation of quark-gluon plasma (QGP) is not expected in proton-proton (pp) and proton-nucleus (pA) collisions due to the absence of a sufficiently large system size and energy density. QGP is formed when a large number of nucleons (protons and neutrons) collide with each other at high energies, creating a system with high energy density and temperature. In pp and pA collisions, the number of nucleons involved in the collision is much smaller than in heavy-ion (AA) collisions, and the energy density and temperature of the system are not sufficient to create a QGP. Additionally, the lifetime of the system created in pp and pA collisions is too short to allow for the formation and evolution of the QGP. Hence, QGP formation is not expected in pp and pA collisions. It is required to compare the measurements in heavy-ion collisions with those from proton-proton (pp) and proton-nucleus (pA) collisions at similar energies for passing a confirmatory statement of QGP formation in heavy-ion collisions. Several physical observables have been studied to provide information about the formation of quark-gluon plasma (QGP) in a system, such as jet quenching, Heavy quark suppression, Dilepton production, Elliptic flow, Strangeness enhancement, etc [14] [11] [15] [5]. These probes are sensitive to different aspects of the QGP.

1.1   Jet production and jet medium interaction

In this thesis, the underlying study is about the strength of the interactions between the jet and the medium.

In high-energy collisions, when the outgoing parton from the hard partonic interaction possesses a large momentum transfer, typically characterized by a significant value of Q^2 (the square of the momentum transfer), it initiates a process known as parton showering. This occurs when the Q^2 is greater than the characteristic energy scale λ_{QCD} associated with strong interactions. Parton showering manifests as a sequential emission of additional partons (quarks or gluons) by the initial parton. These emissions take place in a collimated manner, forming a cascade-like structure. It is worth mentioning that λ_{QCD} denotes the energy scale above which perturbative QCD techniques can be effectively employed to study strong interactions. Eventually, via soft hadronization processes, all partons convert themselves into collimated showers of experimentally detectable hadrons, known as jets. Jets are long-established experimental probes for studies of quantum chromodynamics (QCD) also well described by the theory of perturbative Quantum Chromodynamics (pQCD). Jets lose their energy as they pass through the Quark-Gluon Plasma (QGP) medium through two main mechanisms: gluon radiation and collisional energy loss.

Gluon radiation: It occurs when a fast-moving parton, such as a quark or gluon, interacts with the QGP constituents, which are deconfined quarks and gluons. This is an inelastic interaction of the parton with the medium. The interaction can cause the parton to emit gluons, which carry away energy from the parton and thus reduce its energy. This process is similar to the Bremsstrahlung radiation in QED, where a charged particle emits a photon and loses energy. Gluon radiation is more likely to occur in interactions involving gluons than in interactions involving quarks due to the fact that gluons are bicolored, in contrast to quarks which only carry a single color charge. The probability of gluon radiation increases as the energy of the parton increases due to the larger phase space available for radiation.

The probability of gluon radiation is suppressed for heavy particles due to the reduced phase space available for the emission of radiation.

Collisional energy loss: It occurs when the fast-moving parton collides with the QGP constituents, which can scatter the parton and transfer some of its energy to the QGP constituents. This is an elastic interaction of the parton with the medium. This process is similar to the energy loss of a charged particle in a medium due to Coulomb interactions. The collisional energy loss also depends on the momentum of the parton. Higher momentum partons are less affected by the QGP medium as they spend less time interacting with the medium. Since the collisions are governed by the strong force, which is characterized by a strong coupling constant that increases at low energies or large distances. Therefore, heavy flavor quarks, which have a smaller velocity and larger mass compared to light flavor quarks, experience more frequent and stronger interactions with the QGP constituents, leading to a larger collisional energy loss.

Both gluon radiation and collisional energy loss lead to a reduction in the energy of the jet. As a result, the jet becomes broader in transverse momentum and more diffuse in its particle distribution. The amount of energy loss depends on the properties of the QGP, such as its density, temperature, and viscosity, as well as on the energy and type of the parton that produces the jet. The measurement of jet quenching and jet shape modification, due to the interaction with QGP, provides a powerful tool for studying the properties of the QGP and for testing the predictions of theoretical models.

In the regime of soft gluon emission, the ordering of parton energy loss is predicted to follow the pattern: $\Delta E_b^{rad} < \Delta E_c^{rad} < \Delta E_{u,d}^{rad} < \Delta E_g^{rad}$, as stated in the reference [13]. This ordering also applies to jet modification or jet quenching. According to perturbative QCD (pQCD) calculations, heavy quarks are expected to experience less energy loss in the quark-gluon plasma (QGP) compared to light quarks and gluons [16]. Consequently, beauty quark-initiated jets are anticipated to be less suppressed than light

quark-initiated jets, while gluon-initiated jets are expected to undergo the highest degree of modification.

1.2 Partonic medium in pp collision

Although the formation of a Quark-Gluon Plasma (QGP) in proton-proton (pp) and proton-nucleus (pA) collisions is not expected due to the low energy density reached in such collisions. However, in rare cases, high-multiplicity events can occur in these collisions, which exhibit some features that are similar to those observed in heavy-ion collisions where a QGP is formed.

In high multiplicity proton-proton (pp) collisions, the effects of multi-parton interactions (MPI) and color reconnection (CR) become significant. MPI refers to the scattering of multiple partons in the colliding protons which leads to the higher partonic density, while CR refers to the exchange of color charges between partons from different proton fragments. The presence of MPI and CR can lead to several experimental signatures in high multiplicity pp collisions. These include:

Increased production of strange hadrons: MPI and CR can enhance the production of strange hadrons, as the additional partonic interactions provide more opportunities for these particles to be produced.

Broadening of transverse momentum spectra: The presence of MPI and CR can lead to additional transverse momentum transfers between partons, resulting in a broader transverse momentum distribution of the produced particles. Modification of jet properties: MPI and CR can modify the properties of jets produced in pp collisions, such as their fragmentation patterns and angular distributions.

Overall, the observation of these signatures in high multiplicity pp collisions suggests that the underlying physics is similar to that of heavy-ion collisions, and may be indicative of the formation of a small QGP droplet. However, further studies and measurements are needed to confirm the existence and properties of this QGP-like state in pp collisions.

Chapter 2

2 Pythia Simulation and Analysis Methodology

This section begins by providing an overview of the evolution of proton-proton (pp) collisions within the framework of the PYTHIA event generator. Subsequently, the focus shifts to discussing the chosen physical observable for the study of jet shape, namely the differential jet shape variable $\rho(r)$. Furthermore, an explanation of the jet-matching mechanism employed in this analysis is presented, which enables the matching of a jet with its corresponding initiating parton. In addition to the investigation of the differential jet shape distribution, the effects of multiple parton interactions (MPI) and color reconnection (CR) on jets in pp collisions are also explored through the study of azimuthal angle correlations of the final state charged hadrons with respect to the jet axis(leading hadron). This study is detailed in Appendix 1.

2.1 PYTHIA

The event sample used in this study is generated using PYTHIA 8 Monash 2013 tune (default tune for pp/ppbar). In Pythia8, the proton-proton collision is modeled as a series of sub-processes [7].

1. Hard scattering process: It is characterized by a large momentum transfer or by the exchange of high-energy virtual particles between the colliding partons. The outgoing parton (high pT particle) from the hard scattering produces a collimated shower of partons through parton branch-
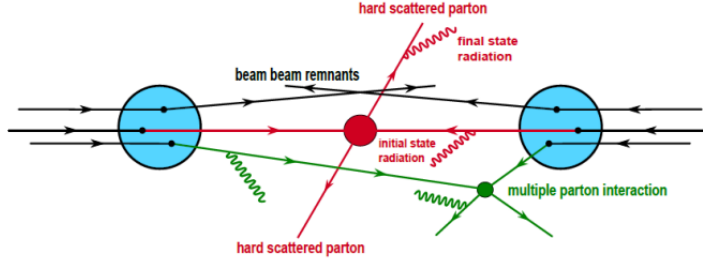
Figure 1: Constituents of Proton-Proton collision

ings. Eventually, all partons convert themselves into collimated showers of experimentally detectable hadrons, known as jets.

2. Multiple parton interactions (MPI): Pythia 8 includes the modeling of multiple parton interactions (MPI), where additional parton-parton interactions occur within the same collision. Due to the MPI the no. of partons participating in hadronization increases which leads to an increased multiplicity of particles and a broader distribution of transverse momentum.
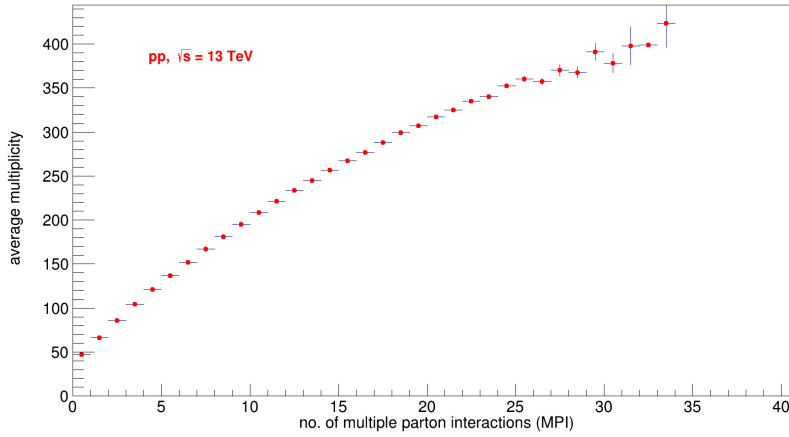
Figure 2: no. of partonic interactions vs average multiplicity

3. Color reconnection (CR) and Hadronization: Partons from hard scattering, MPI and beam remnants are correlated due to color reconnection mechanism. This is because the color strings of the different portions may overlap in space which leads to a reduction in string length. The hadronization process is governed by the lund string fragmentation model in pythia

6

and eventually, the effect of CR reflects in the reduction of hadronic multiplicity.
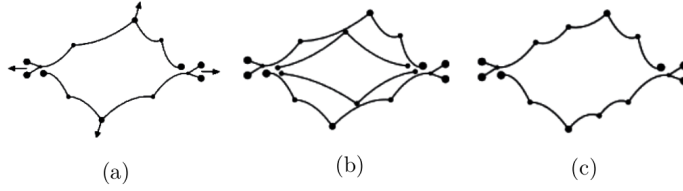
Figure 3: Color Reconnection (CR) mechanism (a) The color connection between the hard scattered partons and the beam remnants. (b) outgoing partons of two hard scatterings are connected to the beam remnants. (c) overlapping of color strings leads to the color reconnection [6].

Overall, Pythia8 provides a comprehensive simulation of the proton-proton collision, including the various subprocesses and aspects that contribute to the final state particles.

The presence of MPI is expected to affect the evolution of jets from the hard scattered initiator parton to the final state hadrons. Additionally, the fragmentation of independent hard scatterings may become correlated due to the color reconnection mechanism, potentially leading to further modifications of jet properties.

2.2 Observable: differential jet shape $\rho(r)$

Here the study of the effects of MPI and CR on the jets is carried out using the differential jet shape observable $\rho(r)$. $\rho(r)$ provides information about the transverse momentum distribution of the jet inside the jet cone. We utilized the FastJet package [8] to reconstruct jet structures in our study, where only the final state charge hadrons with $p_T > 0.15\ GeV/c$ from PYTHIA are considered as input. So the jet reconstruction is done based on the final state charge hadron information using anti-k_T algorithm with jet resolution parameter R = $\sqrt{(\Delta\eta)^2 + (\Delta\phi)^2}$ = 0.4 [12].

The differential jet shape $\rho(r)$ is related to the radial distribution of jet transverse momentum density inside the jet cone about the jet axis and is

7

defined as:

$$\rho(r)^{total} = \frac{1}{\Delta r} \cdot \frac{1}{N_r} \cdot \frac{1}{p^i_{T,jet}} \sum_{i=1}^{N_r} p^i_{T,hadron}(r - \Delta r/2, r + \Delta r/2)$$

Here $\rho(r)^{total}$: Differential jet shape variable for a single jet directly detected in the experiments.

N_r: Total no of jets contributing in the annular region corresponding to the distance r (in $\eta - \phi$ space) from the jet axis.

$p^i_{T,jet}$: Transverse momentum of the jet.

Jets provided by the Fastjet or detected in the experiments are contaminated with the underlying events. To get the pure jet information we need to subtract the background (underlying event contribution) from the detected jet information. To do the underlying event subtraction, rotate the jet axis in the same pseudorapidity by $\pm\pi/2$ in the azimuthal plane. take the region of the same size as the contaminated jet in $\eta - \phi$ space and find out the transverse momentum fraction density $\rho(r)$ distribution for the underlying events.

$$\rho(r)^{UE} = \frac{1}{\Delta r} \cdot \frac{1}{N_r} \cdot \frac{1}{p^i_{T,jet}} \sum_{i=1}^{N_r} p^i_{T,hadron}(r - \Delta r/2, r + \Delta r/2)$$

In our analysis, $p^i_{T,jet}$ is the total transverse momentum of the ith jet after underlying event correction. Since the transverse momentum of the underlying event is quite less than the jet p_T, so it does not matter much if we use the total p_T of the jet in place of corrected jet p_T. Eventually, we get the differential jet shape distribution for an event sample as

$$\rho(r) = \rho(r)^{total} - \rho(r)^{UE}$$

Our study of jet modification in the presence of MPI and CR is focused on high-multiplicity events, as these are the events where the effect of MPI and CR is most pronounced. The high multiplicity (HM) event class is defined as the top 5 percent of events with the highest multiplicities in the pseudorapidity range $|\eta| < 2.4$.

In this study, a sample of around 600 million minimum bias events of pp collisions at $\sqrt{s} = 13 TeV$ is generated using PYTHIA 8 Monash 2013
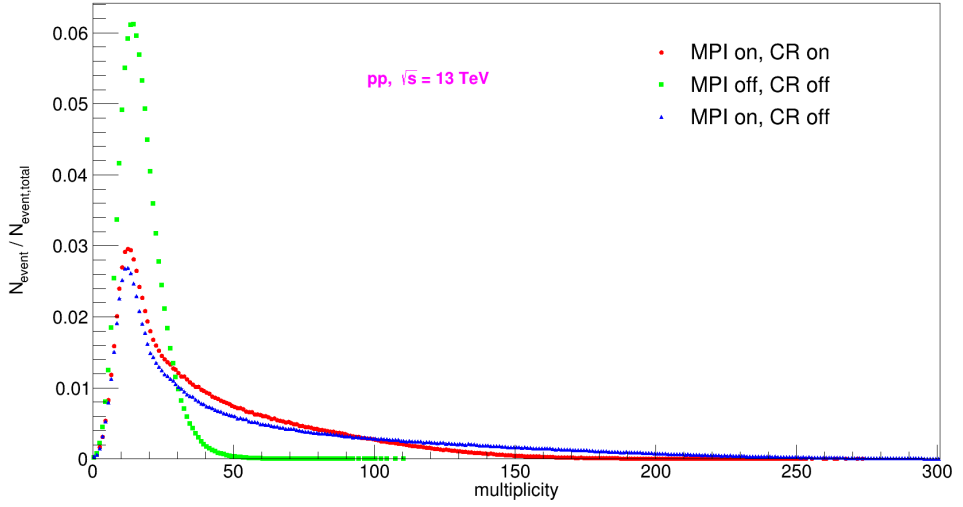
Figure 4: normalized distribution of multiplicity (no. of final state charge hadrons)

event generator. The study considers three different configurations:

1. With both MPI and CR - multiplicity cut 112

2. Without MPI and CR - multiplicity cut 31

3. With MPI and without CR - multiplicity cut 180

The case of MPI off and CR on is not of much interest because, in the absence of MPI, the effect of CR is negligible.

The modification of jet properties may depend on several factors like flavor of the initiator parton, transverse momentum of the jet, pseudorapidity region of the jet study, etc. The study of jet shape variable $\rho(r)$ is done for all types of flavor-initiated jets for two jet transverse momentum ranges $10 < p_{T,jet} < 20$ GeV/c, $50 < p_{T,jet} < 120$ GeV/c. The study of inclusive jets is done for three pseudorapidity ranges $|\eta| < 1$, $1 < |\eta| < 2.5$, $2.5 < |\eta| < 4.5$. The pseudorapidity ranges are decided as per the acceptance of the hadronic calorimeter ($|\eta| < 5$) in CMS detector [10].

2.3   Jet metching Technique

Our focus is on studying the differential jet shape observable that can be measured experimentally. Therefore, we do not delve into the algorithms of jet reconstruction and matching to its initiator proton. Instead, for jet matching, we utilize the partonic level pythia facility.

we start by identifying the outgoing parton from the hardest partonic scattering, which can be either a quark or a gluon. When the outgoing parton is a quark, it undergoes the splitting mode q − > qg. To perform the jet-parton matching, we choose the daughter that shares the same flavor as the initiator quark. This is because the daughter carries most of the quark energy and the least energy is lost to the gluon. If the hard parton is a gluon then we go with it's highest energetic daughter. If there is only one daughter, we choose it directly. We repeat this process multiple times until hadronization occurs. After hadronization, we select the first hadron that contains the same flavor quark from the splitting chain and match it to the jet, which is obtained from the fastjet package, based on the closest distance concept. The jet that is closest to the hadron is then considered to be generated by the parton from the hardest scattering. Therefore, the flavor of this jet's initiator parton is the same as the flavor of the outgoing parton from the hardest scattering.

Chapter 3

3   Results and Analysis

In this section, the analysis focuses on the differential jet shape observable $\rho(r)$ for jets initiated by different types of partons. The study investigates the dependence of $\rho(r)$ for inclusive jets in three pseudorapidity ranges: $|\eta_{\mathrm{jet}}| < 1$, $1 < |\eta_{\mathrm{jet}}| < 2.5$, and $2.5 < |\eta_{\mathrm{jet}}| < 4.5$. Furthermore, the modification of the jet shape is examined for jets initiated by various partons. The impact of multiple parton interactions (MPI) and color reconnection (CR) on the jet shape is also studied by comparing the standard deviation of the spread of the ratio plots for different parton-initiated jets.

3.1   Flavor dependence of differential jet shape $\rho(r)$ distribution

In Figure 5 , the differential jet shape distribution is shown for two jet transverse momentum ranges $10 < p_{T,jet} < 20$ GeV/c (Left) and $50 < p_{T,jet} < 120$ GeV/c (Right). From the figure, it is observed that the high transverse momentum jets are more collimated than the low transverse momentum, the heavy-flavor jets have more spread transverse momentum distribution than the light-flavor jets. The gluonic jets also have a broader jet structure.

Figure 7 is providing information about the splitting angle (angle between the outgoing daughter partons) of the parton under consideration. The splitting angle depends upon the transverse momentum as well as on the flavor of the parton. A high p_T parton has less splitting angle (can be understood physically by the kinematics of the parton decay) than the
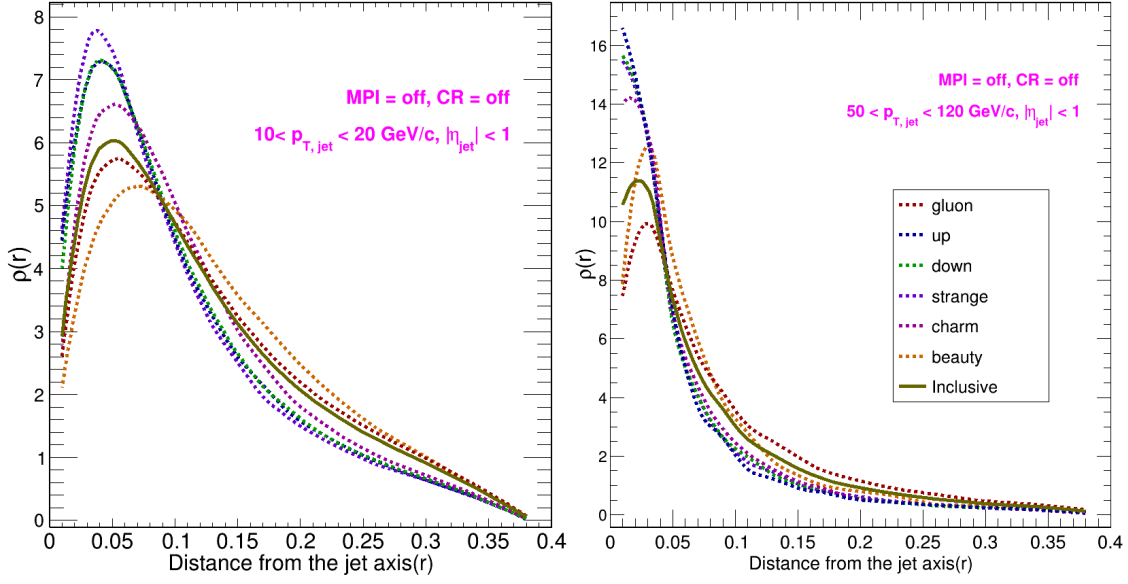
Figure 5: Differential jet shape observable ($\rho(r)$) in the region of $10 < p_{T,jet} < 20$ GeV/c (Left) and $50 < p_{T,jet} < 120$ GeV/c (Right) with $|\eta_{jet}| < 1$, for different parton-initiated jets in the absence of MPI and CR)
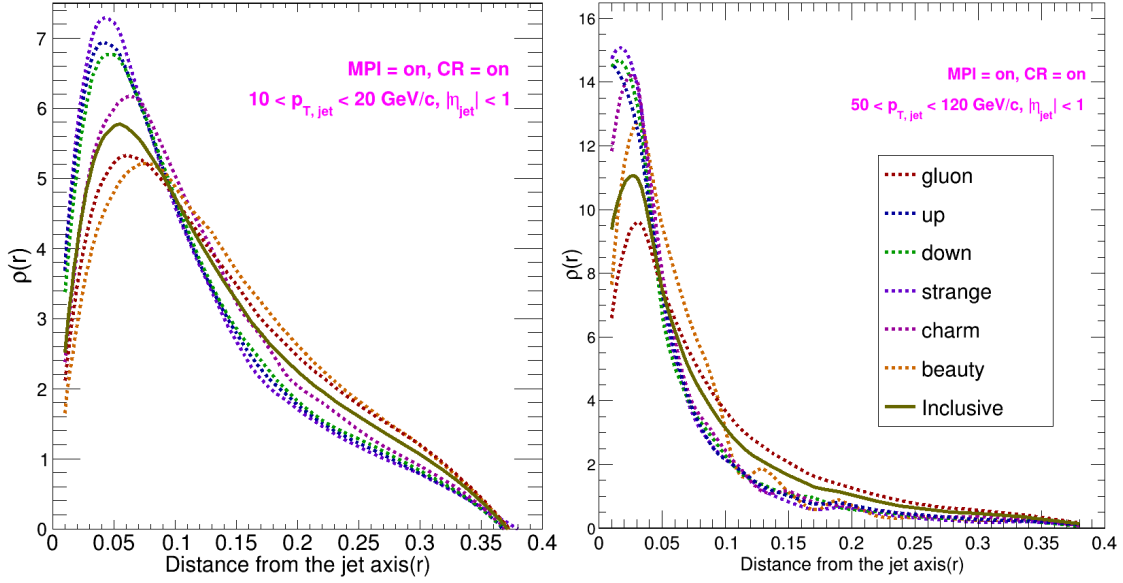
Figure 6: Differential jet shape observable ($\rho(r)$) in the region of $10 < p_{T,jet} < 20$ GeV/c (Left) and $50 < p_{T,jet} < 120$ GeV/c (Right) with $|\eta_{jet}| < 1$, for different parton-initiated jets in the presence of MPI and CR both)

low p_T parton. Also, the heavy flavor quarks have a more splitting angle compared to light flavor quarks at the same transverse momentum. The
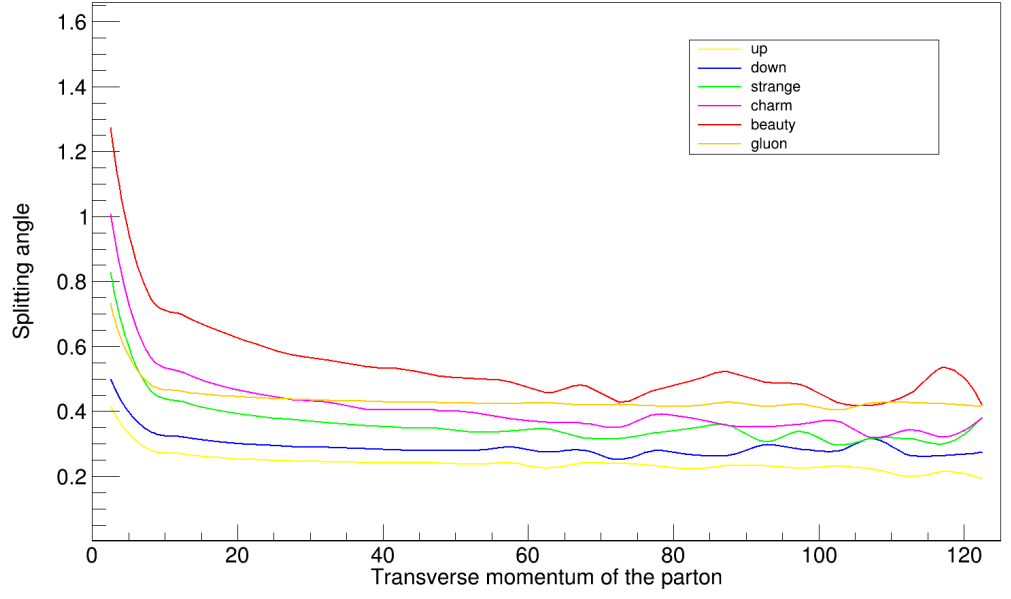
Figure 7: plot between the transverse momentum and the splitting angle of a parton
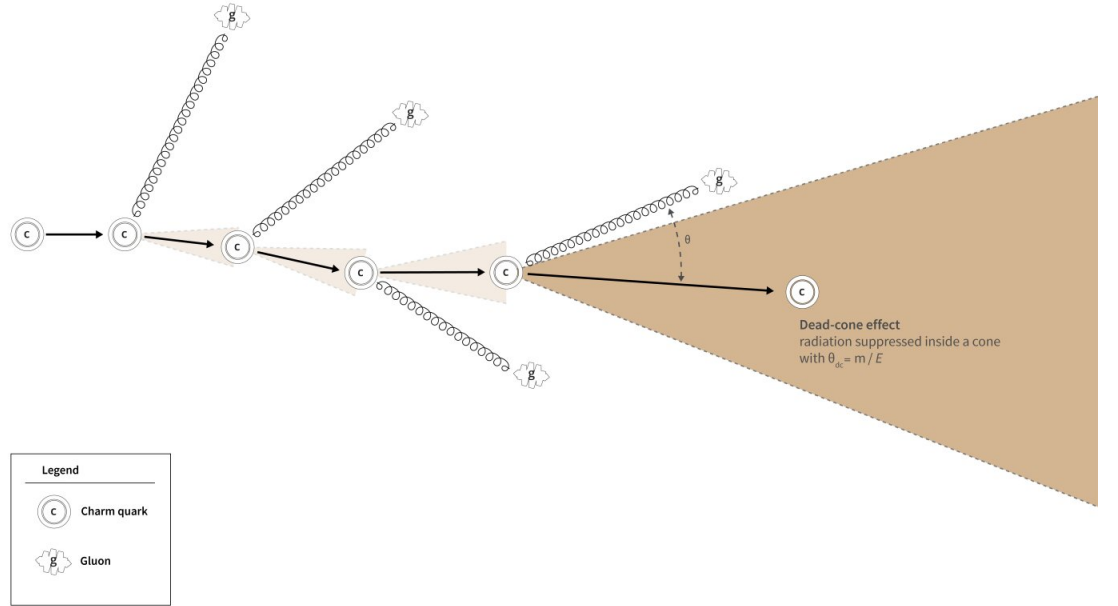
Figure 8: Dead cone effect: Effect of the parton's mass and energy on gluon splitting angle

results depicted in Figure 7 are in agreement with the observations of the Dead Cone effect, as illustrated in Figure 8. The Dead Cone effect involves a restriction on the angle of gluon splitting (relative to the direction of the emitter), which is determined by the mass and energy of the parent parton.

Gluon radiation from an emitter of mass m and energy E is suppressed at angular scales smaller than m/E.

So the flavor and transverse momentum-dependent properties of the jet initiator parton reflect as the different jet shape distributions in the final state.

3.2 Pseudorapidity dependence of differential jet shape $\rho(r)$ distribution
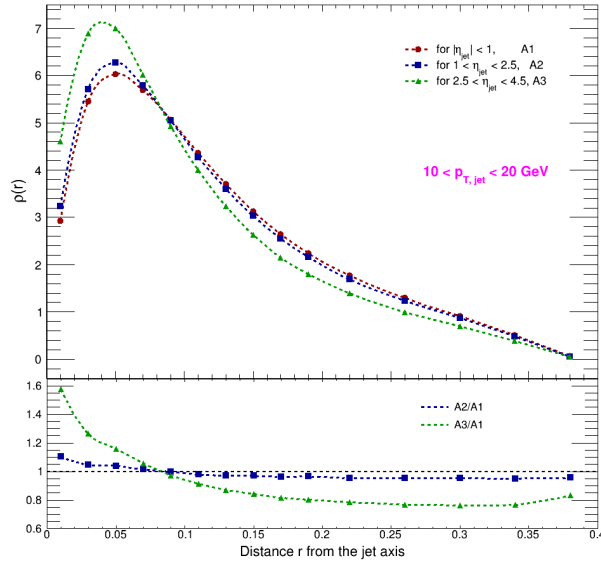
Figure 9: Pseudorapidity dependency of the transverse momentum distribution inside the jet cone as a function of r (distance from the jet axis) for $10 < p_{T,jet} < 20$ GeV/c, MPI and CR both are absent
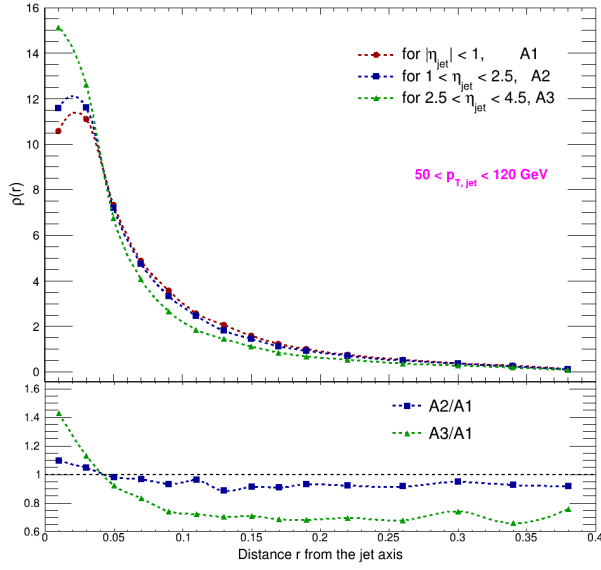
Figure 10: Pseudorapidity dependency of the transverse momentum distribution inside the jet cone as a function of r (distance from the jet axis) for $50 < p_{T,jet} < 120$ GeV/c, MPI and CR both are absent

From Figure 9 and Figure 10, It is clear that in both the jet transverse momentum ranges ($10 < p_{T,jet} < 20$ GeV/c, $50 < p_{T,jet} < 120$ GeV/c), $\rho(r)$ distribution shifts towards the jet axis in the high pseudorapidity region than the mid pseudorapidity region. The justification for this can be given by the kinematics of Proton-Proton (pp) collision. Since in the pp collisions, most of the collision energy goes along the beam axis (at high pseudorapidity range). The high pseudorapidity range contains the particles with high energy and momentum, so when a jet passes through a very high-energy environment then by interacting with the highly energetic partons jets become more collimated by getting some energy from the surrounding.

3.3 Jet shape modification in the presence of MPI and CR mechanisms for the inclusive jets
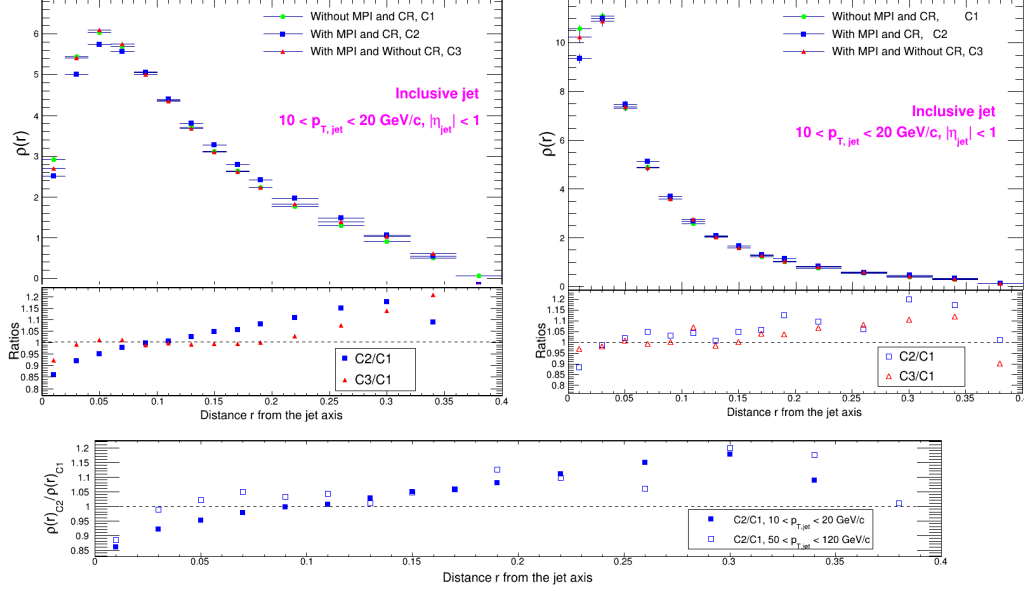
Figure 11: Differential jet shape distribution of the inclusive jets in the pseudorapidity range $|\eta_{jet}| < 1$

If the transverse momentum distribution of the jet is not influenced by the presence of MPI and CR, the ratios plotted in Figure 11 and subsequent figures are expected to remain at 1. A higher deflection observed in the ratio plots from the line at "1" indicates a greater impact of multiple partonic interactions and color reconnection on the jet shape (i.e., transverse momentum distribution inside the jet). Thus, the deviation provides valuable information regarding the sensitivity of the jet shape to MPI and CR.

The findings from Figure 9 demonstrate that MPI and CR have a greater impact on the shape of low transverse momentum jets compared to high transverse momentum jets in mid-pseudorapidity region $|\eta_{jet}| < 1$. It was observed that the jet shape (transverse momentum distribution inside the jet) is less sensitive just to MPI, but is more affected when CR is introduced. A similar type of effect we also got in the forward rapidity region also.

16
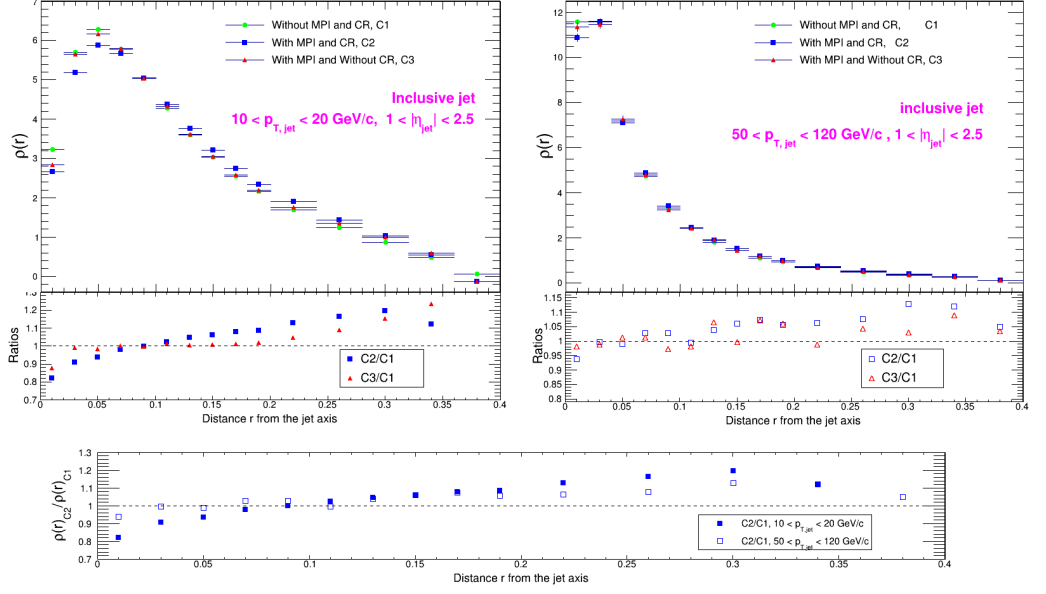
Figure 12: Differential jet shape distribution of the inclusive jets in the pseudorapidity range $1 < |\eta_{jet}| < 2.5$
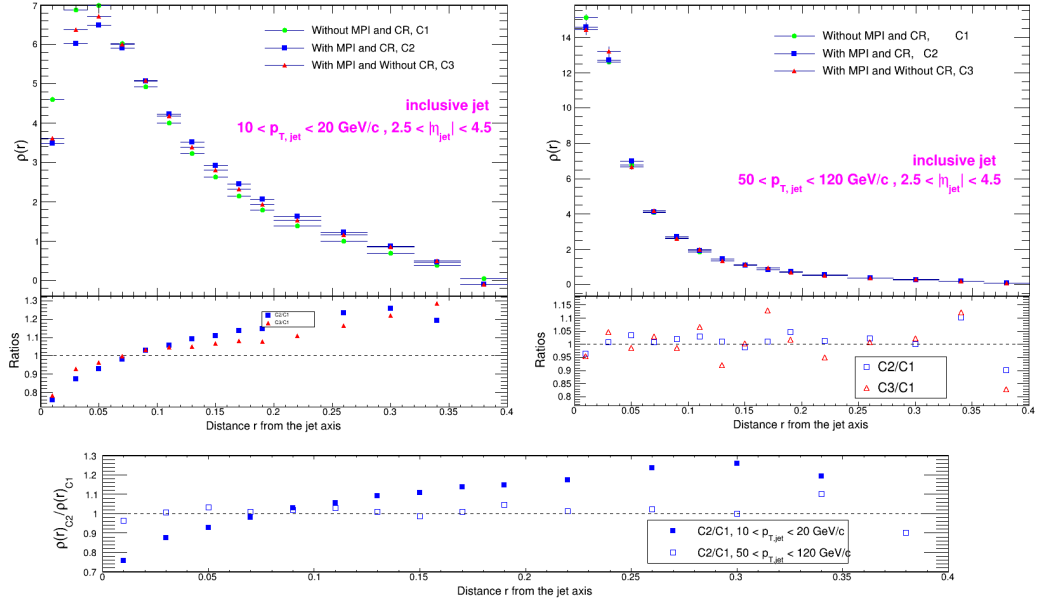
Figure 13: Differential jet shape distribution of the inclusive jets in the pseudorapidity range $2.5 < |\eta_{jet}| < 4.5$
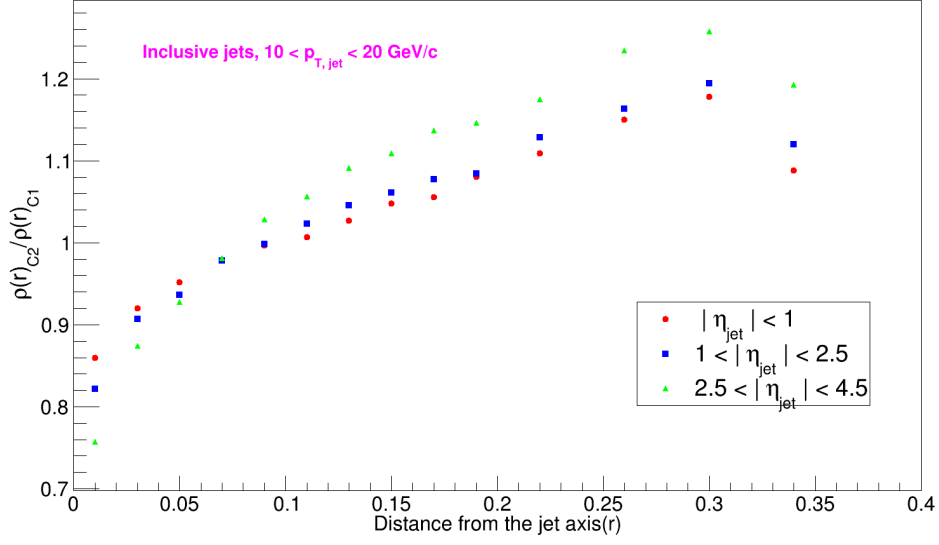
Figure 14: Differential jet shape distribution ratio: $\rho(r)_{\text{with MPI and CR}}$ / $\rho(r)_{\text{without MPI and without CR}}$

The results presented in Figure 14 reveal that the effect of multiple partonic interactions (MPI) and color reconnection (CR) on the jet shape modification is more pronounced in the forward rapidity region as compared to the midrapidity region, especially for low transverse momentum jets.

3.4 Gluon initiated jets in the presence of MPI and CR

The results presented in Figure 15 illustrate the sensitivity of gluonic jets to multiple partonic interactions (MPI) and color reconnection (CR) effects. It is observed that gluonic jets lose their energy dominantly through gluon radiation as they pass through the partonic medium, which leads to the broadening of their transverse momentum distribution. Furthermore, the modification of gluonic jets due to MPI and CR is less significant in the high jet transverse momentum region compared to the low transverse momentum region.
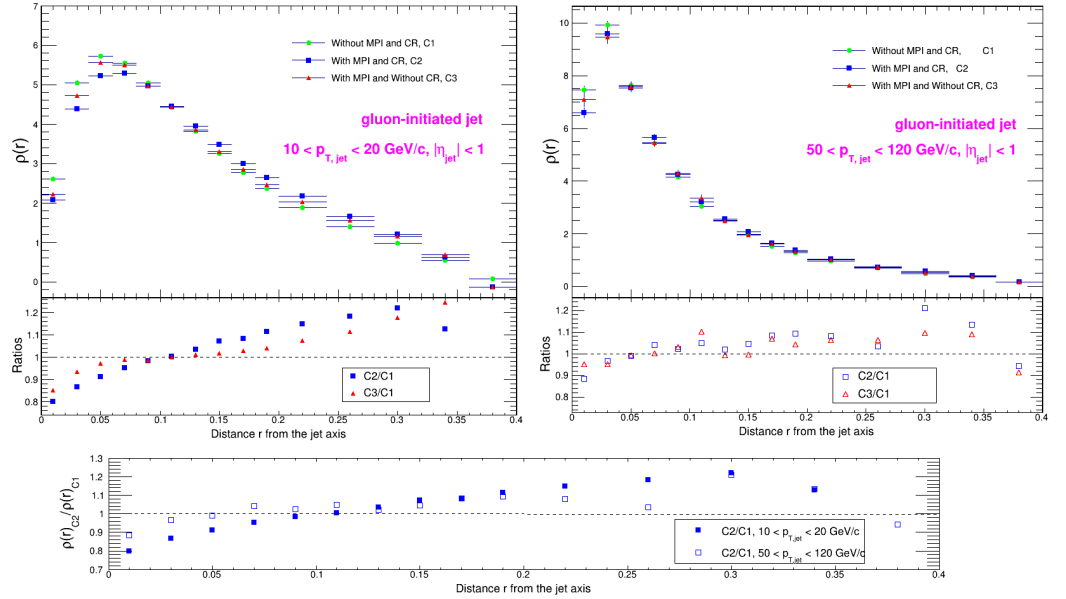
Figure 15: Differential jet shape distribution of the gluonic jets in the pseudorapidity range $|\eta_{jet}| < 1$

3.5 Beauty quark initiated jets in the presence of MPI and CR

The findings depicted in Figure 16 demonstrate the susceptibility of the beauty-initiated jets to the influence of multiple partonic interactions (MPI) and color reconnection (CR) effects.
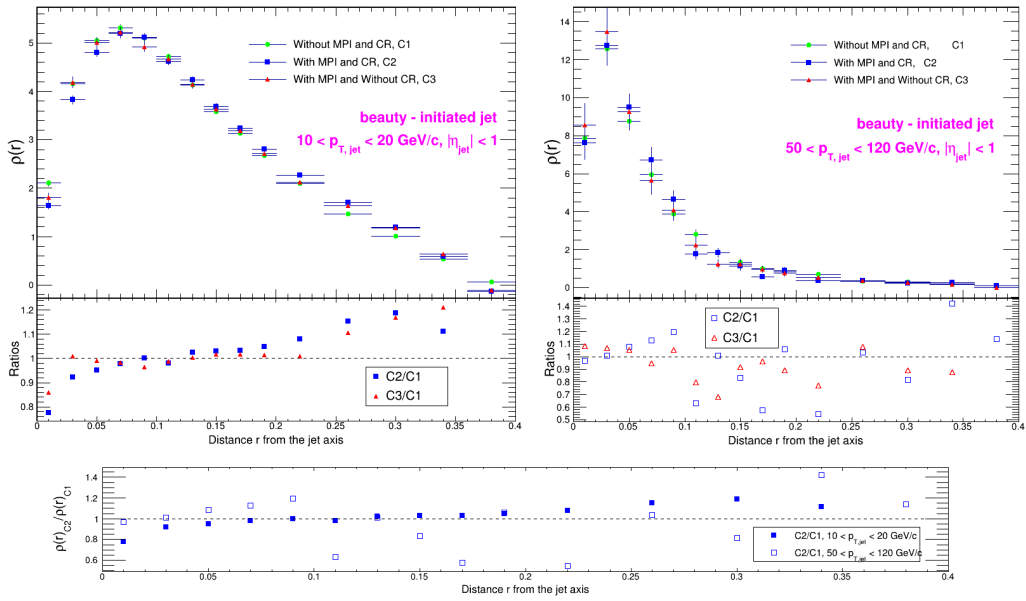
Figure 16: Differential jet shape distribution of the beauty-initiated jets in the pseudorapidity range $|\eta_{jet}| < 1$

3.6 Charm quark initiated jets in the presence of MPI and CR

The results presented in Figure 17 illustrate the sensitivity of charm-initiated jets to multiple partonic interactions (MPI) and color reconnection (CR) effects.
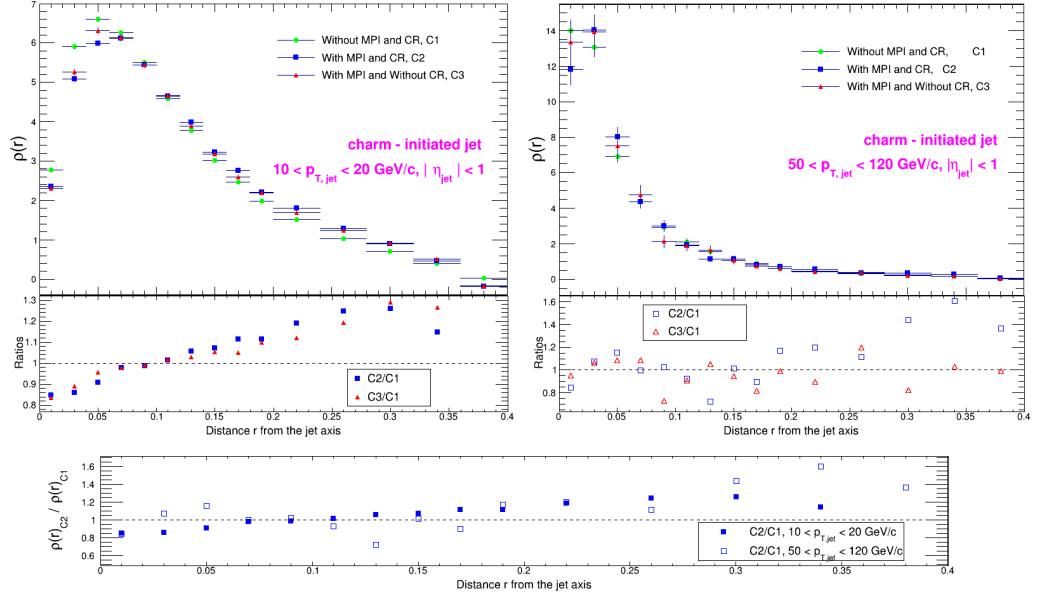
Figure 17: Differential jet shape distribution of the charm quark initiated jets in the pseudorapidity range $|\eta_{jet}| < 1$

3.7 Strange quark initiated jets in the presence of MPI and CR

The results presented in Figure 18 illustrate the sensitivity of strange quark initiated jets to multiple partonic interactions (MPI) and color re-connection (CR) effects.
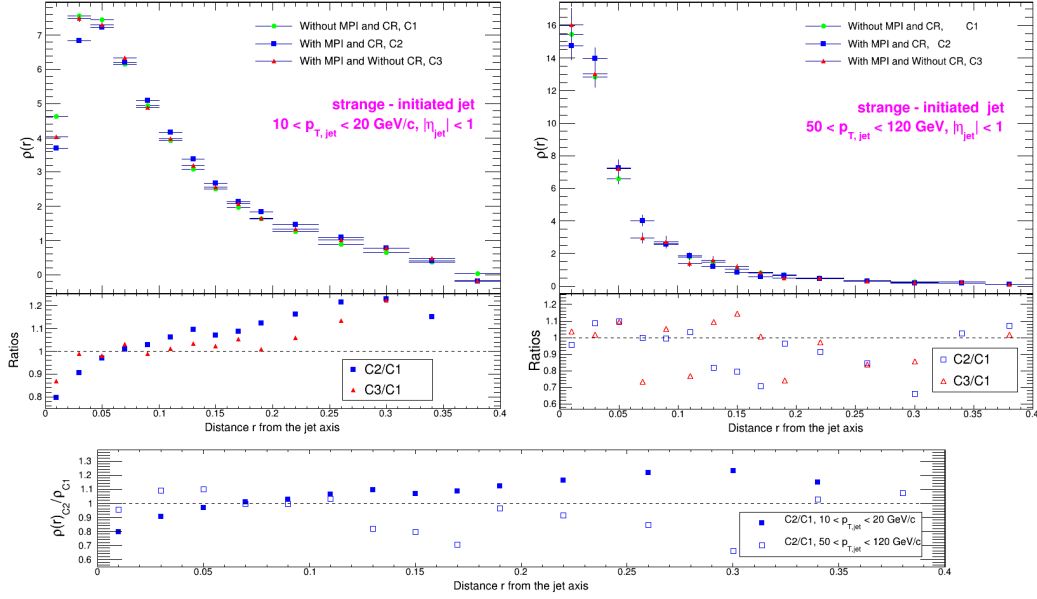
Figure 18: Differential jet shape distribution of the strange quark initiated jets in the pseudorapidity range $|\eta_{jet}| < 1$

3.8 Down quark initiated jets in the presence of MPI and CR

The results presented in Figure 19 illustrate the sensitivity of down quark-initiated jets to multiple partonic interactions (MPI) and color reconnection (CR) effects.
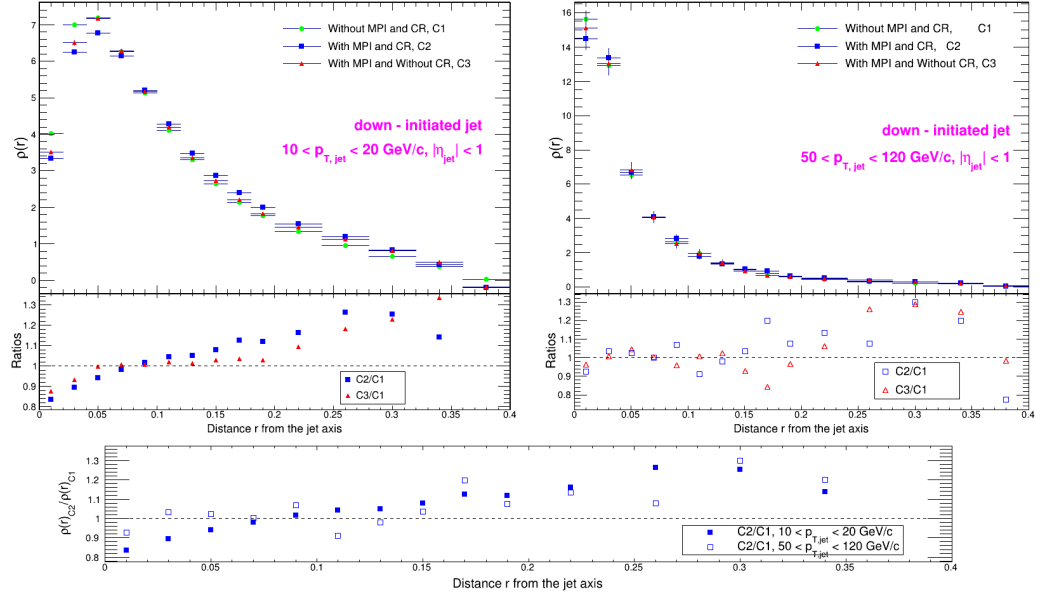
Figure 19: Differential jet shape distribution of the down quark initiated jets in the pseudorapidity range $|\eta_{jet}| < 1$

3.9 Up quark initiated jets in the presence of MPI and CR

The results presented in Figure 20 illustrate the sensitivity of up quark initiated jets to multiple partonic interactions (MPI) and color reconnection (CR) effects.
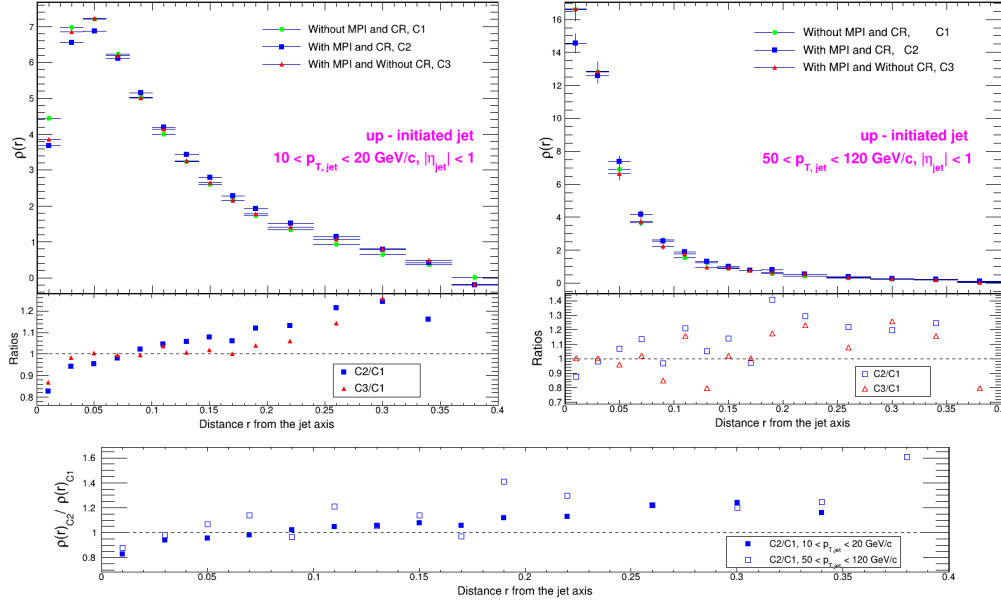
Figure 20: Differential jet shape distribution of the up quark initiated jets in the pseudorapidity range $|\eta_{jet}| < 1$

3.10 Comparision of Jet shape modifications due to the presence of MPI and CR

Figure 21 shows the ratio of the differential jet shape observable for jets initiated by different partons with both MPI and CR enabled, compared to the case when both MPI and CR are disabled. However, due to the overlapping data points, it is difficult to distinguish the specific modifications for each parton-initiated jet.

To address this, in Figure 22, we calculate the standard deviation of the ratio values on the y-axis relative to the ratio equal to 1 line. It is calculated for the first 10 bins (for r < 0.2). This standard deviation provides a measure of the spread or variability in the modifications of different parton-initiated jets. A higher standard deviation indicates a greater modification in the presence of MPI and CR.

From Figure 22, we can observe that gluonic jets exhibit the highest level of modification, with a large standard deviation. On the other hand, beauty-initiated jets show the lowest level of modification, with a smaller standard deviation. Other quark-initiated jets fall between these two extremes.

Additionally, we can infer from Figure 22 that the combined effect of MPI and CR has a greater impact on jet modification compared to the effect of MPI alone. This is evident from the larger standard deviation observed when both MPI and CR are enabled.

Overall, these results provide insights into the modifications of different parton-initiated jets in the presence of MPI and CR, highlighting the varying degrees of sensitivity among different jet types and the enhanced impact of both MPI and CR combined.
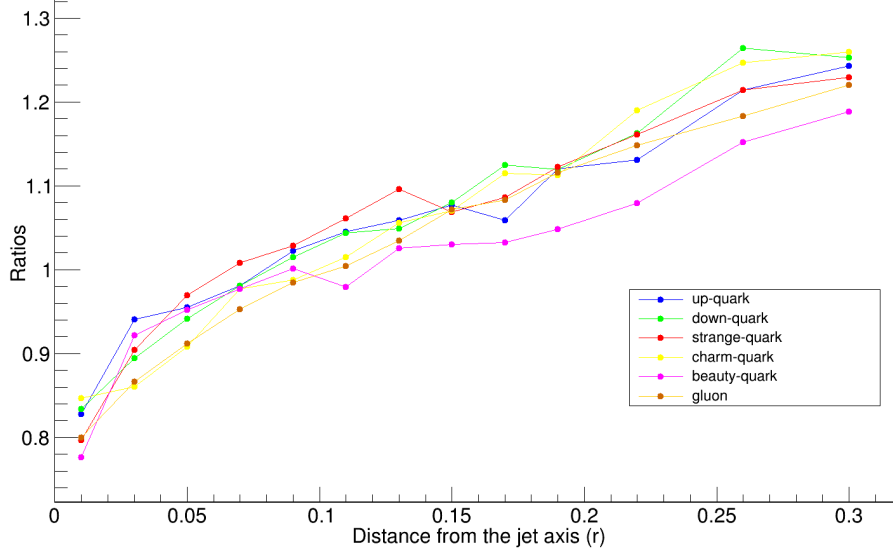
Figure 21: Ratio plot(C2/C1) differential jet shape $\rho(r)$ distribution in with MPI and CR case to the without MPI and without CR case for all type of parton initiated jets
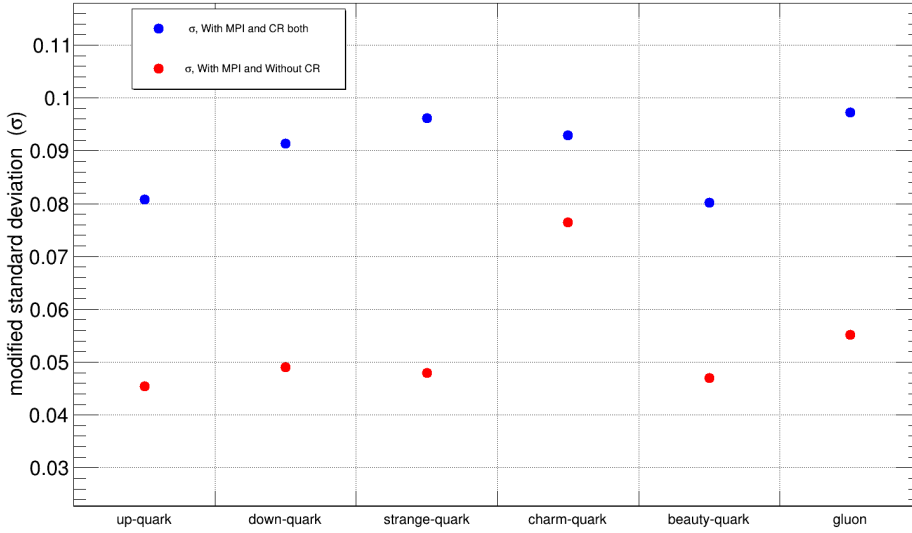
Figure 22: modified standard deviation comparison for different parton initiated jets

Chapter 4

Summary

This thesis presents a comprehensive analysis of the differential jet shape observable $\rho(r)$, examining different flavor-initiated jets across two transverse momentum ranges $10 < p_{T,jet} < 20$ GeV/c and $50 < p_{T,jet} < 120$ GeV/c. The study reveals that heavy-flavor jets have a broader shape compared to light-flavor jets. Gluonic jets also exhibit a broader transverse momentum distribution due to the cascade effect. The effects of multiple parton interactions (MPI) and color reconnection (CR) on the jet shape observable are studied for all types of flavor-initiated jets within the aforementioned transverse momentum ranges at the $|\eta_{jet}| < 1$ pseudorapidity range. The results highlight the sensitivity of the jet shape observable in the presence of only MPI or both MPI and CR. Furthermore, the research investigates the modification of the jet shape for inclusive jets in both central and forward pseudorapidity regions, revealing that forward rapidity jets are more sensitive to MPI and CR compared to mid-rapidity jets at the same jet transverse momentum. Eventually, the study concludes that multiple partonic interactions generate a protonic environment in high-multiplicity pp collisions, affecting various jet properties such as jet fragmentation, jet transverse momentum distribution, etc., when jets pass through this environment.

4 Apendix A: Underlying events and jet shape modification study by using azimuthal angle correlation

In this section, we focus on the analysis of jets and underlying events in relation to the leading particle. The leading particle is characterized as the primary particle [1] having the highest transverse momentum. Therefore, it is anticipated that the hardest scattered parton is the progenitor of the leading particle. Consequently, the leading particle is expected to be closely aligned with the direction of the leading jet.

4.1 Distribution of azimuthal plane with respect to the leading particle direction

Taking into account the sensitivity of the different-different components of a proton-proton collision in different-different regions, the azimuthal plane is divided into the following three regions relative to the leading particle.

Toward Region: Region with $|\Delta\phi| = |\phi_{ch} - \phi_{leading}| < \pi/3$

Away Region: Region with $|\Delta\phi| = |\phi_{ch} - \phi_{leading}| > 2\pi/3$

Transverse Region: Region with $\pi/3 < |\Delta\phi| = |\phi_{ch} - \phi_{leading}| < 2\pi/3$

Here the toward and away regions are sensitive for jet creation and the transverse region is sensitive to the underlying event.
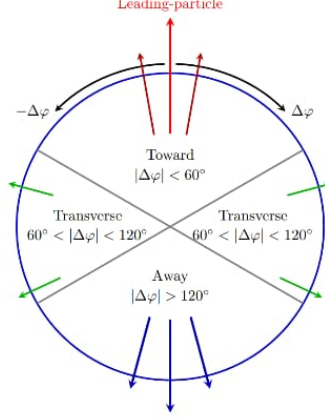
Figure 23: Illustration of the Toward, Away, and Transverse regions in the azimuthal plane with respect to the leading particle direction [3]

The detector imposes certain kinematic constraints to ensure accurate measurements of observable quantities for primary particles. Therefore, In light of the need for comparison, we focus our analysis on primary charged particles within the following constraints: pseudorapidity $|\eta| < 0.8$ and transverse momentum $pT > 0.15$ GeV/c [3]. By adhering to these restrictions, we ensure consistency in the measurement and analysis of observable quantities.

4.2 Dependency of $N_{ch}/N_{ev}(\Delta\eta\Delta\phi)$ and $\Sigma pT/N_{ev}(\Delta\eta\Delta\phi)$ on $pT_{leading}$ and comparison of the model predictions with the ALICE data

Here

N_{ch} = primary charged particle multiplicity

pT = transverse momentum of the primary particle

N_{eV} = number of events

$N_{ch}/N_{ev}(\Delta\phi\Delta\eta)$ = average primary charged particle multiplicity density per event in a specified range of $\Delta\eta$ and $\Delta\phi$

$\Sigma pT/N_{ev}(\Delta\phi\Delta\eta)$ = average total transverse momentum density of primary charged particles per event in a specified range of $\Delta\eta$ and $\Delta\phi$

for all 3 regions $\Delta\eta = 1.6$ and $\Delta\phi = 2\pi/3$

Transverse Region

Figure 24: N_{ch} (left) and Σ pT (right) distributions as a function of $pT_{leading}$ along with the model simulations in the transverse region for the threshold of $pT > 0.15$ GeV/c [3]

The transverse region is particularly sensitive to the underlying events (UE), which include multiple parton interactions (MPI), beam-beam remnants (BBR), and some contributions from initial state radiation (ISR). Figure 24 illustrates that both the number of charged particles (N_{ch}) and the sum of transverse momenta (ΣpT) exhibit a rapid increase at lower values of pT_{leading}, followed by a flattening of the distributions.

Figure 25 demonstrates a similar behavior for the number of parton interactions under MPI (left) and the total transverse momentum of outgoing partons under MPI, as a function of pT_{leading}. It is observed that these quantities also become nearly constant when pT_{leading} approaches 5 GeV/c, indicating the saturation of MPI contributions within the UE.

While Figure 23 represents the combined effects of MPI, ISR, and BBR in shaping the UE, the focus here is primarily on the influence of MPI. Although ISR and BBR contribute to the overall UE, their impact is relatively minor compared to MPI.
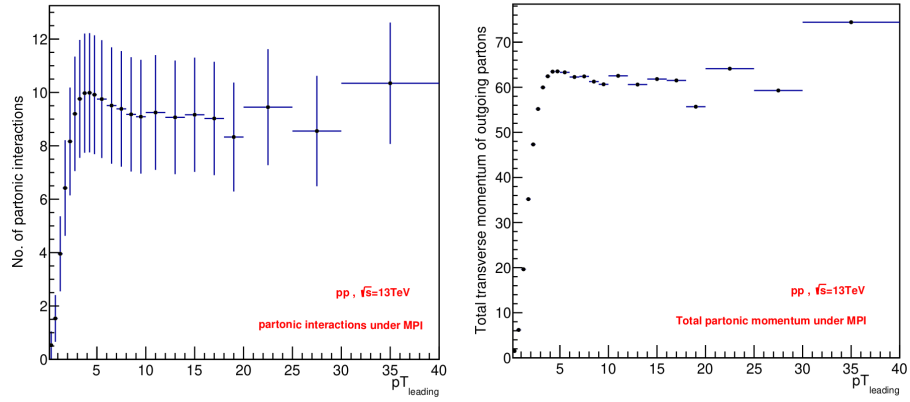
Figure 25: Number of parton parton interactions under MPI (left) and Total transverse momentum of the outgoing partons under MPI in a pp collision as a function of $pT_{leading}$ (GeV/c).

Toward Region

In the toward region, both the number density of charged particles (N_{ch}) and the total transverse momentum density (ΣpT) exhibit a nearly monotonic increase with pT_{leading}. The toward region encompasses contributions

31
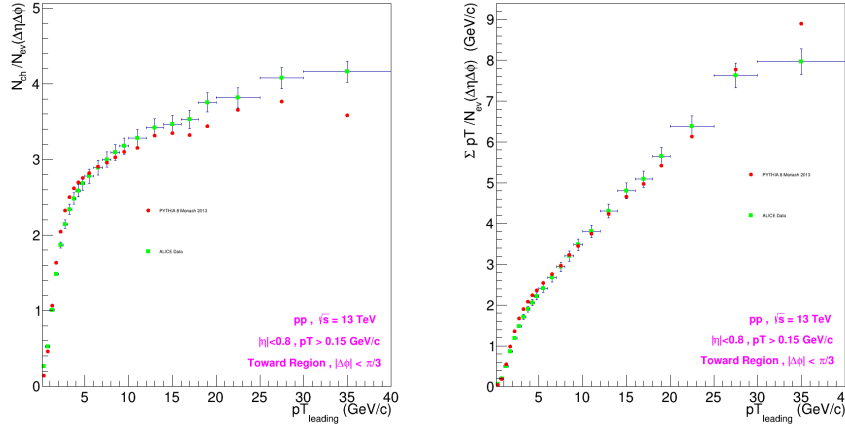
Figure 26: N_{ch} (left) and Σ pT (right) distributions as a fuction of $pT_{leading}$ along with the model simulations in toward region for the threshold of pT > 0.15 GeV/c, contribution of leading particle is excluded[3].

from both the jet (representative of the hard-scattered outgoing parton) and the underlying event, although the dominant component in this region is the jet.

Since the contribution of the underlying event becomes saturated at a specific value of pT_{leading}. Consequently, in Figure 26, the slope is lower at high pT_{leading} values compared to the lower pT_{leading} values, primarily due to the saturation of MPI contributions.

Away Region In away region the shape of Number density N_{ch} (left)

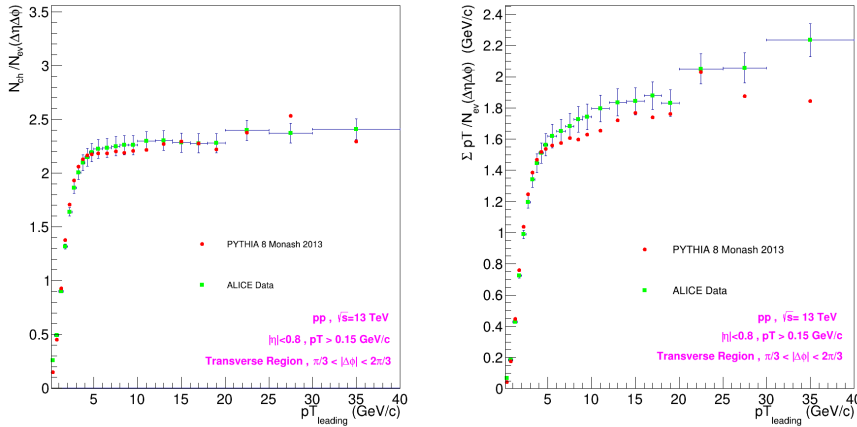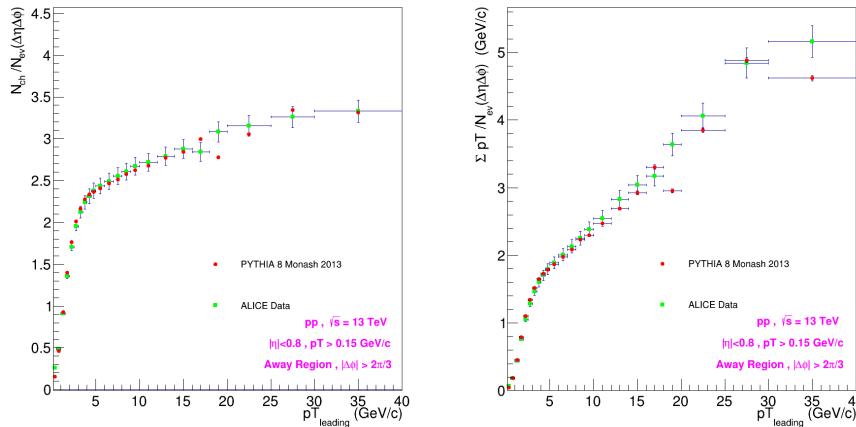Figure 27: N_{ch} (left) and Σ pT (right) distributions as a fuction of $pT_{leading}$ along with the model simulations in away region for the threshold of pT > 0.15 GeV/c [3]

32

and Σ pT (right) distributions are almost similar to the toward region but the magnitude is less than toward region. The reason may be that in toward region we can be almost sure that it contains some jet structure. Due to that we get enhanced N_{ch} and ΣpT. But in away region we can't be always sure that it contains any jet structure. Because the hard scattered outgoing partons are emitted back to back due to momentum conservation. But after the parton branching they may change their directions. So it may happen that we have a jet structure in toward region but not in away region.

4.3 Effect of MPI and Color Reconnection phenomenas on charged particle multiplicity(N_{ch}) distribution
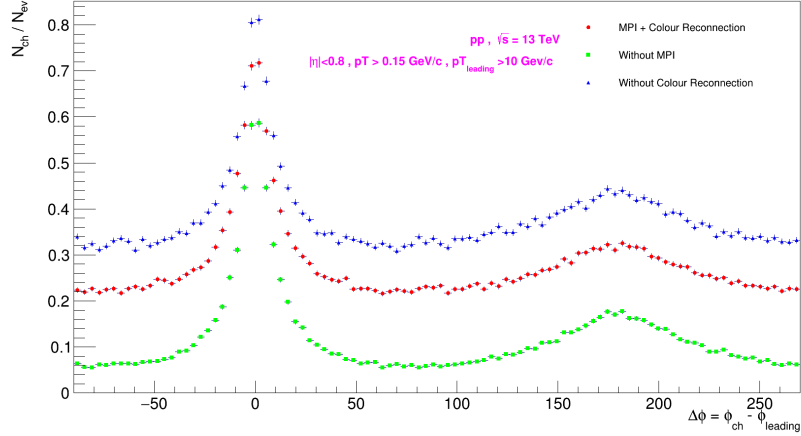
Figure 28: Charged particle multiplicity distribution with respect to $\Delta\phi = \phi_{ch} - \phi_{leading}$, leading particle is excluded

Figure 28 has a cutoff criterion wherein only events with the leading particle transverse momentum greater than 10 GeV/c are considered for analysis. The red plot represent the actual proton-proton collision having contributions from MPI and color reconnection both.

The green one represents the proton-proton collision without MPI, so color reconnection also doesn't contribute. Since MPI is off, the particle multiplicity should reduce, as can be seen in 8.

The blue plot for proton-proton collisions with MPI and without color reconnection has the highest multiplicity.

4.4 Azimuthal angle dependency of the effect of MPI and color reconnection

ΔN_{ch} (N_{ch} **with MPI and CR -** N_{ch} **without MPI)/** N_{ev} **Vs** $\Delta\phi$ **distribution**

Since we know that MPI is a part of the underlying event and it seems that the azimuthal distribution of primary particles created from the underlying event should be almost flat. If we do MPI off, the contribution of the underlying event in N_{ch} should be reduced by an almost constant value independent from the azimuthal angle.

But as shown in Figure 29 , this change is not independent of the azimuthal angle. In the toward region, which aligns with the jet direction,
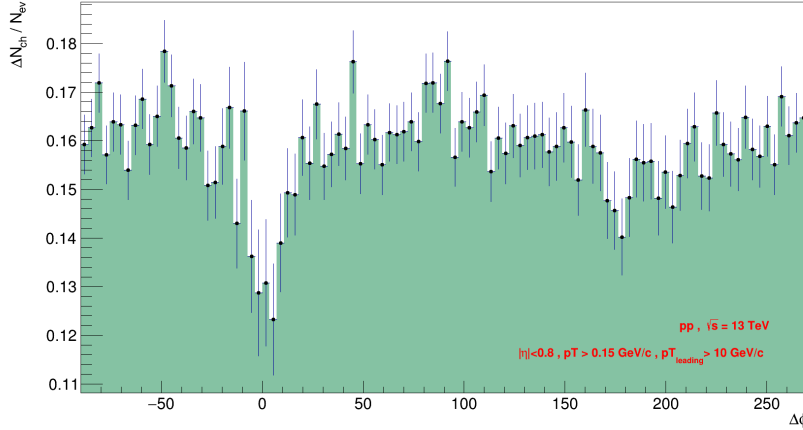
Figure 29: This plot is achieved by subtracting the N_{ch} distribution (green, Figure 28) for the event without MPI from the N_{ch} distribution for the event with MPI and color reconnection (red, Figure 28)

and in the away region, we observe dips in the distribution. These dips indicate a decrease in particle density near $\Delta\phi = 0$ and $\Delta\phi = \pi$. This observation suggests that, in the presence of multiple parton interactions (MPI) and color reconnection (CR), the jets exhibit a broader shape as they

34

lose some energy through interactions with the surrounding medium. Figure 29 illustrates the inclusive jet modification resulting from the presence of multiple parton interactions (MPI) and color reconnection (CR).

ΔN_{ch} (N_{ch} with MPI and without CR - N_{ch} without MPI)/ N_{ev} Vs $\Delta\phi$ distribution

In this scenario, we observe a similar behavior where the jet shape exhibits a dip, but the depth of the dip is less pronounced compared to the previous case. From this observation, we can conclude that multiple parton interactions (MPI) alone can impact the jet shape to some extent, but the combined effect of MPI and color reconnection (CR) is more significant, resulting in a deeper dip in the jet shape distribution
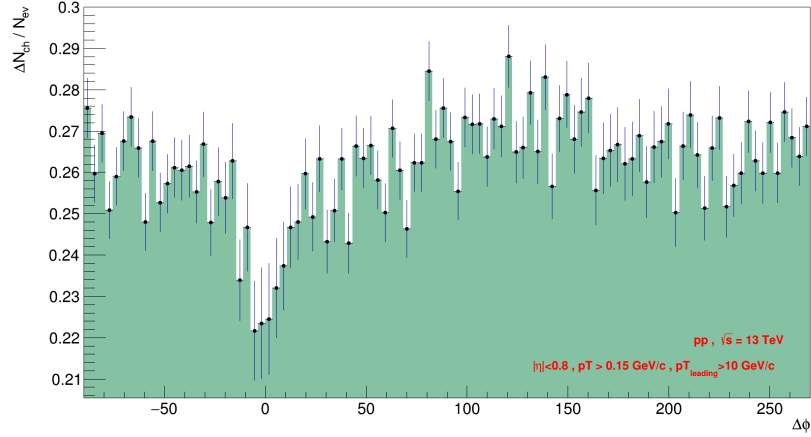
Figure 30: This plot is achieved by subtracting the N_{ch} distribution (blue, Figure 28) for the event without color reconnection from the N_{ch} distribution for the event without MPI (green, Figure 28)

The findings suggest that phenomena such as color reconnection (CR) and underlying event (MPI) have a notable influence on the properties of jets. To gain a better understanding of jet properties in proton-proton (pp) collisions, it becomes imperative to comprehend the specific ways in which jets are impacted by these factors, including the effects of MPI and CR. By studying and analyzing the interplay between jets and these phenomena, we can enhance our understanding of jet behavior and properties in pp collisions.

5 Apendix B: Simulation code for the flavour dependent differential jet shape observable $\rho(r)$

The Simulation code (written in C++) is included in the thesis in 9 parts. It contains the necessary libraries from Pythia, FastJet, CERN Root, and the standard C++ math library (c.math).

```cpp
1  #include <iostream>
2  #include "fastjet/ClusterSequence.hh"
3  #include"Pythia8/Pythia.h"
4  #include"TFile.h"
5  #include"TProfile.h"
6  #include"cmath"
7  #include"TString.h"
8  #include "Pythia8Plugins/FastJet3.h"
9
10 using namespace std;
11 using namespace Pythia8;
12 using namespace fastjet;
13 Pythia pythia;
14
15 int main(int argc, char* argv[])
16 {
17
18 int Events = 1e7;
19 double R = 0.4;
20 double pTMin = 0;
21 double etaMax =25;
22
23 double_t bins[] = {0.0 , 0.02 , 0.04 , 0.06 , 0.08 , 0.1 , 0.12 , 0.14 , 0.16 , 0.18 , 0.2 , 0.24 , 0.28 , 0.32 , 0.36 , 0.4 };
24
25  Int_t Rseed = atoi(argv[1]);
26 TString FileName=Form("Name_of_the_root_file_%d",Rseed);
27 pythia.readString("Beams:idA=2212");
28 pythia.readString("Beams:idB=2212");
29 pythia.readString("Beams:eCM=13000");
30 pythia.readString("SoftQCD:nonDiffractive=on");
31 pythia.readString(" PartonLevel:MPI=on");
32 pythia.readString("ColourReconnection:reconnect=on");
33 pythia.readString("Random:setSeed = on");
34 pythia.readString(Form("Random:seed = %d",Rseed));
35
36
37 TFile* pf = new TFile( FileName+".root","recreate");
38
39
40 TProfile* ph_u1_1_1 = new TProfile("u1_1_1","u1_1_1",15, bins);    TProfile* ph_u1_2_1 = new TProfile("u1_2_1","u1_2_1",15, bins);
41 |
42 TProfile* ph_d1_1_1 = new TProfile("d1_1_1","d1_1_1",15, bins);    TProfile* ph_d1_2_1 = new TProfile("d1_2_1","d1_2_1",15, bins);
43
44 TProfile* ph_s1_1_1 = new TProfile("s1_1_1","s1_1_1",15, bins);    TProfile* ph_s1_2_1 = new TProfile("s1_2_1","s1_2_1",15, bins);
45
46 TProfile* ph_c1_1_1 = new TProfile("c1_1_1","c1_1_1",15, bins);    TProfile* ph_c1_2_1 = new TProfile("c1_2_1","c1_2_1",15, bins);
47
48 TProfile* ph_b1_1_1 = new TProfile("b1_1_1","b1_1_1",15, bins);    TProfile* ph_b1_2_1 = new TProfile("b1_2_1","b1_2_1",15, bins);
49
50 TProfile* ph_g1_1_1 = new TProfile("g1_1_1","g1_1_1",15, bins);    TProfile* ph_g1_2_1 = new TProfile("g1_2_1","g1_2_1",15, bins);
51
52 TProfile* ph_in1_1_1 = new TProfile("in1_1_1","in1_1_1",15, bins);
```

Figure 31: part 1 of the simulation code

```
52 TProfile* ph_in1_1_1 = new TProfile("in1_1_1","in1_1_1",15, bins);
53 TProfile* ph_in1_2_1 = new TProfile("in1_2_1","in1_2_1",15, bins);
54 TProfile* ph_in1_1_2 = new TProfile("in1_1_2","in1_1_2",15, bins);
55 TProfile* ph_in1_2_2 = new TProfile("in1_2_2","in1_2_2",15, bins);
56 TProfile* ph_in1_1_3 = new TProfile("in1_1_3","in1_1_3",15, bins);
57 TProfile* ph_in1_2_3 = new TProfile("in1_2_3","in1_2_3",15, bins);
58
59
60
61
62 JetDefinition jet_def(antikt_algorithm, R);
63
64 pythia.init();
65
66 for(int i=0;i<Events;i++)
67
68 {
69
70
71 if (!pythia.next()) continue;
72
73 int multiplicity = pythia.event.size();
74
75 vector<PseudoJet> particles;
76
77 for (int z = 0; z < multiplicity; ++z)
78 {
79
80 if (pythia.event[z].isFinal() && pythia.event[z].isHadron() && pythia.event[z].isCharged() && pythia.event[z].pT() > 0.15)
81
82 {
83
84 particles.push_back ( PseudoJet(pythia.event[z].px() , pythia.event[z].py() , pythia.event[z].pz() , pythia.event[z].e() ) );
85
86 }
87
88 }
89
90
91 ClusterSequence cs(particles, jet_def);
92
93 vector<PseudoJet> jets = sorted_by_pt(cs.inclusive_jets(pTMin));
94
95
96 int sum1 =0;
97
98
99 for(int h =0;h< multiplicity ; h++)
100 {
101 int idh = pythia.event[h].id();
102 double pTh = pythia.event[h].pT();
103 int statush = pythia.event[h].status();
```

Figure 32: part 2 of the simulation code

```
103 int statush = pythia.event[h].status();
104 bool hadronh = pythia.event[h].isHadron();
105 int chargeh = pythia.event[h].charge();
106 double etah = pythia.event[h].eta();
107
108 if(chargeh != 0 && statush > 0 && hadronh == 1 && abs(etah) < 2.4 )
109 {
110 sum1 = sum1 +1;
111 }
112 }
113
114
115
116 for(int k=0;k<multiplicity;k++)
117
118 {
119 int idk = pythia.event[k].id();
120 double pTk = pythia.event[k].pT();
121 int statusk = pythia.event[k].status();
122 int d1k = pythia.event[k].daughter1();
123 int d2k = pythia.event[k].daughter2();
124 int d1idk = pythia.event[d1k].id();
125 int d2idk = pythia.event[d2k].id();
126 double d1ek = pythia.event[d1k].e();
127 double d2ek = pythia.event[d2k].e();
128 double d1phik = pythia.event[d1k].phi();
129 double d2phik = pythia.event[d2k].phi();
130 double d1yk = pythia.event[d1k].y();
131 double d2yk = pythia.event[d2k].y();
132 int d1od1k = pythia.event[d1k].daughter1();
133 int d2od1k = pythia.event[d1k].daughter2();
134 int d1od1idk = pythia.event[d1od1k].id();
135 int d2od1idk = pythia.event[d2od1k].id();
136 double d1od1ek = pythia.event[d1od1k].e();
137 double d2od1ek = pythia.event[d2od1k].e();
138 bool d1hadronk = pythia.event[d1k].isHadron();
139 double d1od1phik = pythia.event[d1od1k].phi();
140 double d1od1yk = pythia.event[d1od1k].y();
141 bool d1od1hadronk = pythia.event[d1od1k].isHadron();
142
143
144 if(statusk == -23 && ( abs(idk) == 1 || abs(idk) == 2 || abs(idk) == 3 || abs(idk) == 4 || abs(idk) == 5 || idk == 21 ) )
145 {
146
147
148 double pT_total_UE1 = 0;
149 double pT_total_UE2 = 0;
150 double pT_total;
151 double y_jet;
152 double phi_jet;
153 double eta_jet;
154 double pT_jet;
```

Figure 33: part 3 of the simulation code

```
154 double pT_jet;
155 double R_min =1000;
156 double Rn ;
157
158 if(idk == 21)
159 {
160 double dphik = d1phik - d2phik;
161 if(abs(dphik) > pi ) {dphik = 2*pi - abs(dphik); }
162
163 Rn = sqrt( (d1yk - d2yk)*(d1yk - d2yk) + (dphik)*(dphik) );
164 }
165
166 if( ( d1idk != idk && (abs(idk) == 1 || abs(idk) == 2 || abs(idk) == 3 || abs(idk) == 4 || abs(idk) == 5) && d2k != 0 ) || (idk == 21 && d1ek < d2ek && d2k != 0) )
167 {
168 d1k = d2k;
169
170 d1od1k = pythia.event[d1k].daughter1();
171 d2od1k = pythia.event[d1k].daughter2();
172 d1od1idk = pythia.event[d1od1k].id();
173 d1od1ek = pythia.event[d1od1k].e();
174 d2od1ek = pythia.event[d2od1k].e();
175 d1od1phik = pythia.event[d1od1k].phi();
176 d1od1yk = pythia.event[d1od1k].y();
177 d1hadronk = pythia.event[d1k].isHadron();
178 d1od1hadronk = pythia.event[d1od1k].isHadron();
179
180 }
181 if(d1k ==0 && d2k ==0 && idk == 21) { break; }
182 while(d1hadronk ==0)
183 {
184 if(d1od1hadronk == 1)
185 {
186
187 if(d1od1phik < 0)
188 {
189 d1od1phik = 2*pi - abs(d1od1phik);
190 }
191
192 for(int g1 = 0 ; g1 < jets.size();g1++)
193
194 {
195
196
197 double phi_j1 = jets[g1].phi();  double y_j1 = jets[g1].rapidity();  double pt_j1 = jets[g1].pt();  double eta_j1 = jets[g1].eta();  double dphi_j1 = phi_j1 - d1od1phik;
198
199 if (abs(dphi_j1) > pi )
200 {
201 dphi_j1 = 2*pi - abs(dphi_j1);
202 }
203
204
205 double R_jet = sqrt( (y_j1 - d1od1yk)*(y_j1 - d1od1yk) + (dphi_j1)*(dphi_j1) );
```

Figure 34: part 4 of the simulation code

```
205 double R_jet = sqrt( (y_j1 - d1od1yk)*(y_j1 - d1od1yk) + (dphi_j1)*(dphi_j1) );
206
207 if(R_min > R_jet)
208
209 {
210
211 R_min = R_jet; y_jet = y_j1;  phi_jet = phi_j1;  pT_jet = pt_j1;  eta_jet = eta_j1;
212
213 }
214
215 }
216
217
218
219 double phi1 = phi_jet + pi/2;
220 double phi2 = phi_jet - pi/2;
221
222
223 if(phi1 > 2*pi)
224 {
225 phi1 = phi1 - 2*pi;
226 }
227
228 if(phi2 < 0)
229 {
230 phi2 = 2*pi - abs(phi2) ;
231 }
232
233
234
235 for (int l =0; l< multiplicity; l++)
236 {
237
238 int statusl = pythia.event[l].status();  bool hadronl = pythia.event[l].isHadron();  double phil = pythia.event[l].phi();  double yl = pythia.event[l].y();  double pTl = pythia.event[l].pT();  double
    el = pythia.event[l].e();  int chargel = pythia.event[l].charge();
239
240 if(phil < 0)
241 {
242 phil = 2*pi - abs(phil);
243 }
244
245 double dphi1 = phi1 - phil;
246
247 if(abs(dphi1) > pi)
248 {
249 dphi1 = 2*pi - abs(dphi1);
250 }
251
252 double Rl1 = sqrt( (y_jet - yl)*(y_jet - yl) + (dphi1)*(dphi1) );
253
254 if(chargel != 0 && statusl > 0 && hadronl == 1 &&  pTl > 0.15  && Rl1 < 0.4 )
255 {
```

Figure 35: part 5 of the simulation code

```
255 {
256 pT_total_UE1 = pTl + pT_total_UE1;
257 }
258
259 }
260
261
262 for (int l =0; l< multiplicity; l++)
263 {
264
265 int statusl = pythia.event[l].status();  bool hadronl = pythia.event[l].isHadron();  double phil = pythia.event[l].phi();  double yl = pythia.event[l].y();  double pTl = pythia.event[l].pT();  double
    el = pythia.event[l].e();  int chargel = pythia.event[l].charge();
266
267 if(phil < 0)
268 {
269 phil = 2*pi - abs(phil);
270 }
271
272 double dphi2 = phi2 - phil;
273
274 if(abs(dphi2) > pi)
275 {
276 dphi2 = 2*pi - abs(dphi2);
277 }
278
279 double Rl2 = sqrt( (y_jet - yl)*(y_jet - yl) + (dphi2)*(dphi2) );
280
281 if(chargel != 0 && statusl > 0 && hadronl == 1 &&  pTl > 0.15  && Rl2 < 0.4 )
282 {
283 pT_total_UE2 = pTl + pT_total_UE2;
284 }
285
286 }
287
288 pT_total = pT_jet - 0.5*pT_total_UE1 - 0.5*pT_total_UE2 ;
289
290 if(pT_total > 0.2*pTk )
291 {
292
293
294 for(int m =0; m< 15 ; m++)
295 {
296
297 double pT_0 = 0;   double pT_1 = 0;   double pT_2 = 0;
298
299 if(m< 10)
300 {
301
302 for (int l =0; l< multiplicity; l++)
303 {
304
305 int statusl = pythia.event[l].status();  double phil = pythia.event[l].phi();  double yl = pythia.event[l].y();  double pTl = pythia.event[l].pT();  double el = pythia.event[l].e();  int chargel =
```

Figure 36: part 6 of the simulation code

```
384
385 int statusl = pythia.event[l].status();  double phil = pythia.event[l].phi();  double yl = pythia.event[l].y();  double pTl = pythia.event[l].pT();  double el = pythia.event[l].e();  int chargel =
    pythia.event[l].charge();  bool hadronl = pythia.event[l].isHadron();
386
307 if(phil < 0) { phil = 2*pi - abs(phil); }
388
309 double dphi = phi_jet - phil;
310 if(abs(dphi) > pi) { dphi = 2*pi - abs(dphi); }
311 double Rl0 = sqrt( (y_jet - yl)*(y_jet - yl) + (dphi)*(dphi) );
312
313 double dphi1 = phil1 - phil;
314 if(abs(dphi1) > pi) { dphi1 = 2*pi - abs(dphi1); }
315 double Rl1 = sqrt( (y_jet - yl)*(y_jet - yl) + (dphi1)*(dphi1) );
316
317 double dphi2 = phi2 - phil;
318 if(abs(dphi2) > pi) { dphi2 = 2*pi - abs(dphi2); }
319 double Rl2 = sqrt( (y_jet - yl)*(y_jet - yl) + (dphi2)*(dphi2) );
320
321 if(chargel != 0 && statusl > 0 && hadronl == 1 && pTl > 0.15  && Rl0 > 0.02*m && Rl0 < 0.02*(m+1) ) { pT_0 = pT_0 + pTl; }
322 if(chargel != 0 && statusl > 0 && hadronl == 1 && pTl > 0.15  && Rl1 > 0.02*m && Rl1 < 0.02*(m+1) ) { pT_1 = pT_1 + pTl; }
323 if(chargel != 0 && statusl > 0 && hadronl == 1 && pTl > 0.15  && Rl2 > 0.02*m && Rl2 < 0.02*(m+1) ) { pT_2 = pT_2 + pTl; }
324
325 }
326
327 double pT_R = pT_0 - 0.5*pT_1 - 0.5*pT_2;
328 double pT_RF = pT_R / pT_total;
329 double pT_RFD = 50*pT_RF;
330 double t = m*0.02 + 0.01;
331
332 if( abs(idk) == 1 && pT_total > 10 && pT_total < 20  && sum1 > 180 && abs(eta_jet) < 1)                { ph_d1_1_1 ->Fill( t,pT_RFD); }
333 if( abs(idk) == 1 && pT_total > 50 && pT_total < 120 && sum1 > 180 && abs(eta_jet) < 1)                { ph_d1_2_1 ->Fill( t,pT_RFD); }
334
335 if( abs(idk) == 2 && pT_total > 10 && pT_total < 20  && sum1 > 180 && abs(eta_jet) < 1)                { ph_u1_1_1 ->Fill( t,pT_RFD); }
336 if( abs(idk) == 2 && pT_total > 50 && pT_total < 120 && sum1 > 180 && abs(eta_jet) < 1)                { ph_u1_2_1 ->Fill( t,pT_RFD); }
337
338 if( abs(idk) == 3 && pT_total > 10 && pT_total < 20  && sum1 > 180 && abs(eta_jet) < 1)                { ph_s1_1_1 ->Fill( t,pT_RFD); }
339 if( abs(idk) == 3 && pT_total > 50 && pT_total < 120 && sum1 > 180 && abs(eta_jet) < 1)                { ph_s1_2_1 ->Fill( t,pT_RFD); }
340
341 if( abs(idk) == 5 && pT_total > 10 && pT_total < 20  && sum1 > 180 && abs(eta_jet) < 1)                { ph_b1_1_1 ->Fill( t,pT_RFD); }
342 if( abs(idk) == 5 && pT_total > 50 && pT_total < 120 && sum1 > 180 && abs(eta_jet) < 1)                { ph_b1_2_1 ->Fill( t,pT_RFD); }
343
344 if( abs(idk) == 4 && pT_total > 10 && pT_total < 20  && sum1 > 180 && abs(eta_jet) < 1)                { ph_c1_1_1 ->Fill( t,pT_RFD); }
345 if( abs(idk) == 4 && pT_total > 50 && pT_total < 120 && sum1 > 180 && abs(eta_jet) < 1)                { ph_c1_2_1 ->Fill( t,pT_RFD); }
346
347 if( idk == 21 && pT_total > 10 && pT_total < 20  && sum1 > 180 && abs(eta_jet) < 1)                { ph_g1_1_1 ->Fill( t,pT_RFD); }
348 if( idk == 21 && pT_total > 50 && pT_total < 120 && sum1 > 180 && abs(eta_jet) < 1)                { ph_g1_2_1 ->Fill( t,pT_RFD); }
349
350 if( pT_total > 10 && pT_total < 20  && sum1 > 180 && abs(eta_jet) < 1)                { ph_in1_1_1 ->Fill( t,pT_RFD); }
351 if( pT_total > 50 && pT_total < 120 && sum1 > 180 && abs(eta_jet) < 1)                { ph_in1_2_1 ->Fill( t,pT_RFD); }
352 if( pT_total > 10 && pT_total < 20  && sum1 > 180 && abs(eta_jet) > 1   && abs(eta_jet) < 2.5)  { ph_in1_1_2 ->Fill( t,pT_RFD); }
353 if( pT_total > 50 && pT_total < 120 && sum1 > 180 && abs(eta_jet) > 1   && abs(eta_jet) < 2.5)  { ph_in1_2_2 ->Fill( t,pT_RFD); }
354 if( pT_total > 10 && pT_total < 20  && sum1 > 180 && abs(eta_jet) > 2.5 && abs(eta_jet) < 4.5)  { ph_in1_1_3 ->Fill( t,pT_RFD); }
```

Figure 37: part 7 of the simulation code

```
354 if( pT_total > 10 && pT_total < 20  && sum1 > 180 && abs(eta_jet) > 2.5 && abs(eta_jet) < 4.5)   { ph_in1_1_3 ->Fill( t,pT_RFD); }
355 if( pT_total > 50 && pT_total < 120 && sum1 > 180 && abs(eta_jet) > 2.5 && abs(eta_jet) < 4.5)   { ph_in1_2_3 ->Fill( t,pT_RFD); }
356 }
357
358
359
360 if(m > 9 && m < 15 )
361 {
362
363 for (int l =0; l< multiplicity; l++)
364 {
365
366 int statusl = pythia.event[l].status();  double phil = pythia.event[l].phi();  double yl = pythia.event[l].y();  double pTl = pythia.event[l].pT();  double el = pythia.event[l].e();  int chargel =
    pythia.event[l].charge();  bool hadronl = pythia.event[l].isHadron();
367
368 if(phil < 0) { phil = 2*pi - abs(phil); }
369
370 double dphi = phi_jet - phil;
371 if(abs(dphi) > pi) { dphi = 2*pi - abs(dphi); }
372 double Rl0 = sqrt( (y_jet - yl)*(y_jet - yl) + (dphi)*(dphi) );
373
374 double dphi1 = phi1 - phil;
375 if(abs(dphi1) > pi) { dphi1 = 2*pi - abs(dphi1); }
376 double Rl1 = sqrt( (y_jet - yl)*(y_jet - yl) + (dphi1)*(dphi1) );
377
378 double dphi2 = phi2 - phil;
379 if(abs(dphi2) > pi) { dphi2 = 2*pi - abs(dphi2); }
380 double Rl2 = sqrt( (y_jet - yl)*(y_jet - yl) + (dphi2)*(dphi2) );
381
382 if(chargel != 0 && statusl > 0 && hadronl == 1 && pTl > 0.15  && Rl0 > (0.04*m - 0.2) && Rl0 < (0.04*m - 0.16) )  { pT_0 = pT_0 + pTl; }
383 if(chargel != 0 && statusl > 0 && hadronl == 1 && pTl > 0.15  && Rl1 > (0.04*m - 0.2) && Rl1 < (0.04*m - 0.16) )  { pT_1 = pT_1 + pTl; }
384 if(chargel != 0 && statusl > 0 && hadronl == 1 && pTl > 0.15  && Rl2 > (0.04*m - 0.2) && Rl2 < (0.04*m - 0.16) )  { pT_2 = pT_2 + pTl; }
385
386 }
387
388 double pT_R = pT_0 - 0.5*pT_1 - 0.5*pT_2;
389 double pT_RF = pT_R / pT_total;
390 double pT_RFD = 25*pT_RF;
391 double t = m*0.04 - 0.19;
392
393 if( abs(idk) == 1 && pT_total > 10 && pT_total < 20  && sum1 > 180 && abs(eta_jet) < 1)                        { ph_d1_1_1 ->Fill( t,pT_RFD); }
394 if( abs(idk) == 1 && pT_total > 50 && pT_total < 120 && sum1 > 180 && abs(eta_jet) < 1)                        { ph_d1_2_1 ->Fill( t,pT_RFD); }
395
396 if( abs(idk) == 2 && pT_total > 10 && pT_total < 20  && sum1 > 180 && abs(eta_jet) < 1)                        { ph_u1_1_1 ->Fill( t,pT_RFD); }
397 if( abs(idk) == 2 && pT_total > 50 && pT_total < 120 && sum1 > 180 && abs(eta_jet) < 1)                        { ph_u1_2_1 ->Fill( t,pT_RFD); }
398
399 if( abs(idk) == 3 && pT_total > 10 && pT_total < 20  && sum1 > 180 && abs(eta_jet) < 1)                        { ph_s1_1_1 ->Fill( t,pT_RFD); }
400 if( abs(idk) == 3 && pT_total > 50 && pT_total < 120 && sum1 > 180 && abs(eta_jet) < 1)                        { ph_s1_2_1 ->Fill( t,pT_RFD); }
401
402 if( abs(idk) == 5 && pT_total > 10 && pT_total < 20  && sum1 > 180 && abs(eta_jet) < 1)                        { ph_b1_1_1 ->Fill( t,pT_RFD); }
403 if( abs(idk) == 5 && pT_total > 50 && pT_total < 120 && sum1 > 180 && abs(eta_jet) < 1)                        { ph_b1_2_1 ->Fill( t,pT_RFD); }
404
```

Figure 38: part 8 of the simulation code

```
403 if( abs(idk)  == 3 && pT_total > 50 && pT_total < 120 && sum1 > 180 && abs(eta_jet) < 1)          { ph_s1_2_1 ->Fill( t,pT_RFD); }
404
405 if( abs(idk) == 4 && pT_total > 10 && pT_total < 20  && sum1 > 180 && abs(eta_jet) < 1)                      { ph_c1_1_1 ->Fill( t,pT_RFD); }
406 if( abs(idk) == 4 && pT_total > 50 && pT_total < 120 && sum1 > 180 && abs(eta_jet) < 1)                      { ph_c1_2_1 ->Fill( t,pT_RFD); }
407
408 if( idk == 21 && pT_total > 10 && pT_total < 20  && sum1 > 180 && abs(eta_jet) < 1)                      { ph_g1_1_1 ->Fill( t,pT_RFD); }
409 if( idk == 21 && pT_total > 50 && pT_total < 120 && sum1 > 180 && abs(eta_jet) < 1)                      { ph_g1_2_1 ->Fill( t,pT_RFD); }
410
411 if( pT_total > 10 && pT_total < 20  && sum1 > 180 && abs(eta_jet) < 1)                        { ph_in1_1_1 ->Fill( t,pT_RFD); }
412 if( pT_total > 50 && pT_total < 120 && sum1 > 180 && abs(eta_jet) < 1)                        { ph_in1_2_1 ->Fill( t,pT_RFD); }
413 if( pT_total > 10 && pT_total < 20  && sum1 > 180 && abs(eta_jet) > 1   && abs(eta_jet) < 2.5)  { ph_in1_1_2 ->Fill( t,pT_RFD); }
414 if( pT_total > 50 && pT_total < 120 && sum1 > 180 && abs(eta_jet) > 1   && abs(eta_jet) < 2.5)  { ph_in1_2_2 ->Fill( t,pT_RFD); }
415 if( pT_total > 10 && pT_total < 20  && sum1 > 180 && abs(eta_jet) > 2.5 && abs(eta_jet) < 4.5)  { ph_in1_1_3 ->Fill( t,pT_RFD); }
416 if( pT_total > 50 && pT_total < 120 && sum1 > 180 && abs(eta_jet) > 2.5 && abs(eta_jet) < 4.5)  { ph_in1_2_3 ->Fill( t,pT_RFD); }
417
418
419 }
420 }
421 }
422 }
423
424 if( ( d1od1hadronk == 0 && d1od1idk != idk && (abs(idk) == 1 || abs(idk) == 2 || abs(idk) == 3 || abs(idk) == 4 || abs(idk) == 5) && d2od1k != 0 ) || (d1od1hadronk == 0 && d1od1ek < d2od1ek &&
    d2od1k != 0 && idk ==21 ) )
425 {
426 d1od1k = d2od1k;
427 }
428
429 if(d1od1hadronk == 0 && d1od1k == 0 &&  d2od1k == 0 && idk == 21 )
430 {
431 break;
432 }
433
434 d1k = d1od1k;
435 d1idk = pythia.event[d1k].id();
436 d1od1k = pythia.event[d1k].daughter1();
437 d2od1k = pythia.event[d1k].daughter2();
438 d1od1idk = pythia.event[d1od1k].id();
439 d1hadronk = pythia.event[d1k].isHadron();
440 d1od1ek = pythia.event[d1od1k].e();
441 d2od1ek = pythia.event[d2od1k].e();
442 d1od1hadronk = pythia.event[d1od1k].isHadron();
443 d1od1phik = pythia.event[d1od1k].phi();
444 d1od1yk = pythia.event[d1od1k].y();
445
446 }
447 }
448 }
449 }
450
451 pf->Write();
452 pf->Close();
453 return 0;
454 }
```

Figure 39: part 9 of the simulation code

Bibliography

[1] The ALICE definition of primary particles. 2017.

[2] K. Aamodt et al. Suppression of charged particle production at large transverse momentum in central pb–pb collisions at snn=2.76 tev. *Physics Letters B*, 696(1):30–39, 2011.

[3] Shreyasi Acharya et al. Underlying Event properties in pp collisions at $\sqrt{s} = 13$ TeV. *JHEP*, 04:192, 2020.

[4] J. Adams et al. Evidence from $d + $ Au measurements for final-state suppression of high-p_T hadrons in Au $+$ Au collisions at rhic. *Phys. Rev. Lett.*, 91:072304, Aug 2003.

[5] Madan Aggarwal. *Elliptic Flow in Relativistic Heavy-Ion Collisions*, pages 161–188. 01 2021.

[6] ALICE Collaboration. "Number density and Sum p_T , pT > 0.15 GeV/c " of "Underlying Event properties in pp collisions at $\sqrt{s} = 13$ TeV" (Version 1). HEPData (dataset), 2020. https://doi.org/10.17182/hepdata.94414.v1/t1.

[7] Christian Bierlich, Smita Chakraborty, Nishita Desai, Leif Gellersen, Ilkka Helenius, Philip Ilten, Leif Lönnblad, Stephen Mrenna, Stefan Prestel, Christian T. Preuss, Torbjörn Sjöstrand, Peter Skands, Marius Utheim, and Rob Verheyen. A comprehensive guide to the physics and usage of pythia 8.3, 2022.

[8] Matteo Cacciari, Gavin P. Salam, and Gregory Soyez. FastJet user manual. *The European Physical Journal C*, 72(3), mar 2012.

[9] S. Chatrchyan et al. Jet momentum dependence of jet quenching in pbpb collisions at snn=2.76 tev. *Physics Letters B*, 712(3):176–197, 2012.

[10] The CMS Collaboration. The cms experiment at the cern lhc. *Journal of Instrumentation*, 3(08):S08004, aug 2008.

[11] Megan Connors, Christine Nattrass, Rosi Reed, and Sevil Salur. Jet measurements in heavy ion physics. *Rev. Mod. Phys.*, 90:025005, Jun 2018.

[12] Prottoy Das, Abhi Modak, Debjani Banerjee, Rathijit Biswas, Supriya Das, Sanjay K. Ghosh, Sibaji Raha, and Sidharth Kumar Prasad. Jet modification in absence of qgp-medium: the role of multiparton interactions and color reconnection, 2022.

[13] Hai Tao Li and Ivan Vitev. Inverting the mass hierarchy of jet quenching effects with prompt b-jet substructure. *Physics Letters B*, 793:259–264, 2019.

[14] Fu-Ming Liu and Sheng-Xu Liu. Quark-gluon plasma formation time and direct photons from heavy ion collisions. *Physical Review C*, 89(3), mar 2014.

[15] S. Soff, S.A. Bass, M. Bleicher, L. Bravina, M. Gorenstein, E. Zabrodin, H. Stöcker, and W. Greiner. Strangeness enhancement in heavy ion collisions – evidence for quark-gluon matter? *Physics Letters B*, 471(1):89–96, dec 1999.

[16] Wen-Jing Xing, Shanshan Cao, Guang-You Qin, and Hongxi Xing. Heavy and light flavor jet quenching in heavy-ion collisions in a perturbative QCD approach. *Nucl. Phys. A*, 1005:121829, 2021.